



Article

<https://doi.org/10.1038/s41592-024-02411-6>

A modular chemigenetic calcium indicator for multiplexed *in vivo* functional imaging

Received: 20 July 2023

Accepted: 12 August 2024

Published online: 20 September 2024

Check for updates

Helen Farrants¹✉, Yichun Shuai¹, William C. Lemon¹, Christian Monroy Hernandez¹, Deng Zhang¹, Shang Yang¹, Ronak Patel¹, Guanda Qiao¹, Michelle S. Frei^{1,4,5}, Sarah E. Plutkis¹, Jonathan B. Grimm¹, Timothy L. Hanson¹, Filip Tomaska^{1,6}, Glenn C. Turner¹, Carsen Stringer¹, Philipp J. Keller¹, Abraham G. Beyene¹, Yao Chen¹, Yajie Liang¹, Luke D. Lavis¹ & Eric R. Schreiter¹✉

Genetically encoded fluorescent calcium indicators allow cellular-resolution recording of physiology. However, bright, genetically targetable indicators that can be multiplexed with existing tools *in vivo* are needed for simultaneous imaging of multiple signals. Here we describe WHaloCaMP, a modular chemigenetic calcium indicator built from bright dye-ligands and protein sensor domains. Fluorescence change in WHaloCaMP results from reversible quenching of the bound dye via a strategically placed tryptophan. WHaloCaMP is compatible with rhodamine dye-ligands that fluoresce from green to near-infrared, including several that efficiently label the brain in animals. When bound to a near-infrared dye-ligand, WHaloCaMP shows a 7× increase in fluorescence intensity and a 2.1-ns increase in fluorescence lifetime upon calcium binding. We use WHaloCaMP1a to image Ca^{2+} responses *in vivo* in flies and mice, to perform three-color multiplexed functional imaging of hundreds of neurons and astrocytes in zebrafish larvae and to quantify Ca^{2+} concentration using fluorescence lifetime imaging microscopy (FLIM).

Fluorescent indicators allow non-invasive imaging of cellular physiology in living animals, and genetically encoded fluorescent Ca^{2+} indicators (GECIs) have been especially useful to approximate neuronal activity during behavior^{1–3}. The most widely used GECIs are engineered from fluorescent proteins and emit in the green-to-red region of the visible spectrum. Near-infrared (~670–900 nm) fluorophores can be imaged deeper in tissue due to reduced scattering and multiplexed with existing green and red probes⁴. However, there are limited functional indicators in the near-infrared.

Existing near-infrared fluorescent indicators require either a cofactor or a synthetic small molecule, which poses challenges for *in vivo* use⁵. Near-infrared Ca^{2+} indicators that make use of biliverdin-binding proteins^{6,7} are limited by the availability of biliverdin, a product of heme catabolism in mammalian cells, and have low quantum yields, making *in vivo* imaging with good signal-to-noise ratio challenging. While synthetic small-molecule dyes can be brighter than biliverdin-binding proteins, they must be delivered to the desired tissue. In addition, to achieve genetic targeting, the small-molecule dyes must be selectively

¹Janelia Research Campus, Howard Hughes Medical Institute, Ashburn, VA, USA. ²Department of Neuroscience, Washington University in St. Louis, St. Louis, MO, USA. ³Department of Diagnostic Radiology and Nuclear Medicine, University of Maryland School of Medicine, Baltimore, MD, USA. ⁴Department of Chemical Biology, Max Planck Institute for Medical Research, Heidelberg, Germany. ⁵Present address: Department of Pharmacology, University of California San Diego, La Jolla, CA, USA. ⁶Present address: Department of Electrical and Computer Engineering, Center for BioEngineering, Neuroscience Research Institute, University of California, Santa Barbara, Santa Barbara, CA, USA. ✉e-mail: farrantsh@janelia.hhmi.org; schreitere@janelia.hhmi.org

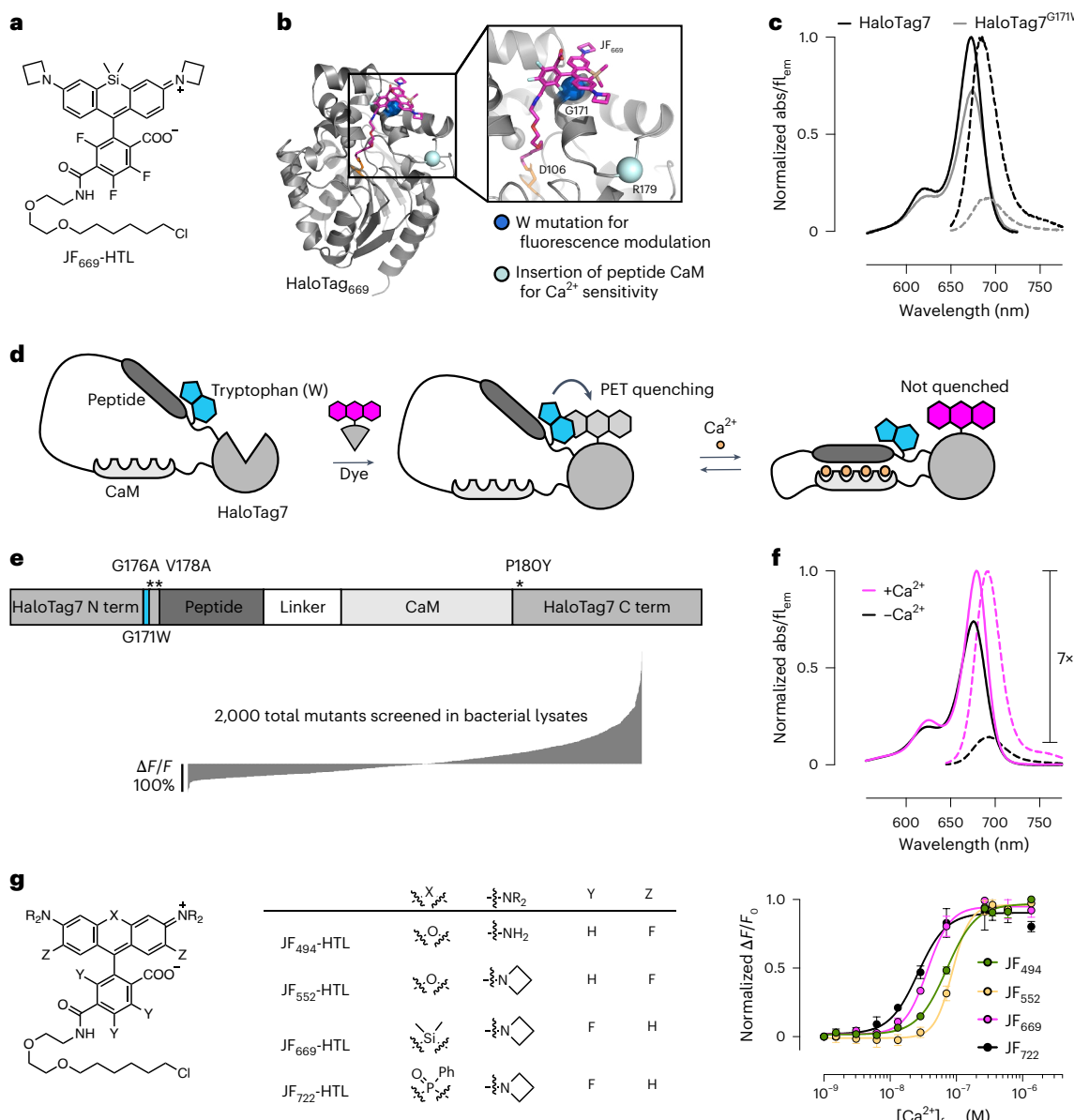


Fig. 1 | Engineering chemigenetic Ca²⁺ indicators with tryptophan quenching. **a**, Chemical structure of the JF₆₆₉-HaloTag ligand (HTL). **b**, Crystal structure of HaloTag7 bound to the JF₆₆₉-HaloTag ligand (HaloTag₆₆₉) (PDB 8SW8). The positions of G171, which was mutated to a tryptophan to quench dye fluorescence emission, and R179, where Ca²⁺-sensitive protein domains were inserted, are highlighted as spheres. **c**, Normalized absorption (abs; solid lines) and fluorescence emission (f_{em} ; dashed lines) spectra of the JF₆₆₉-HaloTag ligand bound to HaloTag7 or the HaloTag^{G171W} mutant. **d**, Schematic representation of WHaloCaMP, showing domain arrangement, covalent binding of the dye-ligand

and the quenching tryptophan. **e**, Primary structure of WHaloCaMP1a (top) and $\Delta F/F_0$ values of variants (bottom) from a bacterial lysate screen to select WHaloCaMP1a. Term, terminus. **f**, Normalized absorption (solid lines) and fluorescence emission (dashed lines) spectra of the JF₆₆₉-HaloTag ligand bound to purified WHaloCaMP1a in the presence (magenta) and absence (black) of Ca²⁺. **g**, Chemical structures of the dye-ligands used here with WHaloCaMP1a (left) and normalized Ca²⁺ titrations of WHaloCaMP1a bound to these dye-ligands (right). Data points represent mean and s.d. from $n = 3$ replicates. [Ca²⁺], Ca²⁺ concentration.

retained by a specific cell type, for example, by using a self-labeling protein⁸. We previously engineered fluorescent indicators⁹ with far-red or near-infrared emission using environmentally sensitive dye-ligands, such as JF₆₃₅-HaloTag ligand¹⁰ and the self-labeling HaloTag protein⁹ in a ‘chemigenetic’ or ‘hybrid’ approach. However, these dye-ligands exhibited limited bioavailability in the central nervous system and the resulting sensors could not be efficiently used for functional imaging in the brains of animals.

Here, we describe chemigenetic Ca²⁺ indicators built from bright dye-ligands for which the fluorescence output is modulated by photoinduced electron transfer (PET) to a protein-based quencher. The modular approach allowed us to use rhodamine dye-ligands with

emission ranging from green to near-infrared, including dye-ligands that efficiently distribute into the central nervous system in animals. We use these sensors to demonstrate imaging of Ca²⁺ responses in flies and mice and perform three-color multiplexed functional imaging as well as quantitative Ca²⁺ FLIM in zebrafish larvae.

Results

Design of the chemigenetic Ca²⁺ indicator WHaloCaMP

To construct a bright, near-infrared chemigenetic Ca²⁺ sensor for use in animals, we focused on the JF₆₆₉-HaloTag ligand (Fig. 1a). This dye-ligand has emission just on the edge of the near-infrared and has previously been reported to efficiently label neurons in mouse brains following

Table 1 | Photophysical properties of WHaloCaMP1a bound to dye-ligands

WHaloCaMP1a	Abs _{apo} (nm)	Abs _{sat} (nm)	Ex/Em _{apo} (nm)	Ex/Em _{sat} (nm)	Dynamic range (F _{max} /F _{min})	K _d (nM)	Hill coeff.	ε _{apo} (×1,000) (M ⁻¹ cm ⁻¹)	ε _{sat} (×1,000) (M ⁻¹ cm ⁻¹)	Φ _{apo}	Φ _{sat}	Brightness _{apo} (mM ⁻¹ cm ⁻¹)	Brightness _{sat} (mM ⁻¹ cm ⁻¹)
JF ₄₉₄ -HTL	505	502	504/524	502/522	10	71±3	1.9±0.1	138	144	<0.05	0.20	N.D.	28.8
JF ₅₅₂ -HTL	561	562	559/578	565/582	4	87±5	3.1±0.7	73	78	0.05	0.25	3.6	19.5
JF ₆₆₉ -HTL	675	678	677/688	679/690	7	37±2	2.5±0.3	127	174	0.08	0.50	10.1	87.0
JF ₇₂₂ -HTL	726	730	728/743	732/748	16	26±2	2.0±0.3	99	119	<0.05	0.16	N.D.	19.0

The quantum yield was too low to be measured. Abs, absorbance; apo, in presence of EGTA; max, maximum; min, minimum; sat, in presence of saturating Ca²⁺; Ex, excitation maximum; Em, emission maximum; K_d, estimated dissociation constant for Ca²⁺ or half-maximum effective concentration (EC₅₀) from titration curves; Hill coeff., Hill coefficient; ε, molar extinction coefficient; Φ, quantum yield; brightness (mM⁻¹cm⁻¹), the product of molar extinction coefficient×quantum yield divided by 1,000; N.D., not determined.

intravascular injection^{11,12}. We did not concentrate on environmentally sensitive dye-ligands such as JF₆₃₅-HaloTag ligand, which we previously used to engineer the HaloCaMP chemogenetic Ca²⁺ indicators, as we could not detect the JF₆₃₅-HaloTag ligand in the central nervous system of mice following vascular injection. Fluorescence changes in the HaloCaMP sensors relied on modulating the environment of the dyes via protein conformational changes driven by Ca²⁺ binding. The environmental sensitivity of rhodamine dyes is characterized by the equilibrium between the nonfluorescent lactone and the fluorescent zwitterionic forms. In previous work^{10,11,13}, we found that the lactone–zwitterion equilibrium constant (K_{L-Z}) of a rhodamine dye is a descriptor that largely predicts both bioavailability in the central nervous system and the environmental sensitivity of dye-ligand derivatives (Supplementary Note 1). Unfortunately, the optimal range of K_{L-Z} for bioavailability shows little overlap with the optimal range for environmental sensitivity. Thus, the excellent bioavailability of the JF₆₆₉-HaloTag ligand is at the expense of environmental sensitivity; this dye-ligand does not exhibit large Ca²⁺-dependent fluorescence changes when used with the previously published HaloCaMP sensors (Supplementary Fig. 1).

Instead of tuning the lactone–zwitterion equilibrium to find a dye with suboptimal bioavailability and environmental sensitivity, we hypothesized that we could generate Ca²⁺-binding-induced fluorescence changes via reversible quenching of the dye by tryptophan from the protein through PET. Tryptophan mutants of HaloTag have previously been used to quench the fluorescence of rhodamine dyes¹⁴ and to improve the dynamic range of fluorescent indicators¹⁵. To guide our engineering efforts, we solved the crystal structure of the JF₆₆₉-HaloTag ligand bound to HaloTag7 (Fig. 1b, Protein Data Bank (PDB) 8SW8 and Supplementary Table 1) and found that G171 was within the required spatial distance of ~5 Å for fluorescence quenching through PET¹⁶. Mutating G171 on HaloTag7 to a tryptophan decreased fluorescence emission of bound JF₆₆₉ by 85% (Fig. 1c), providing a way to strongly modulate the dye fluorescence emission.

We next sought to couple the fluorescence quenching of HaloTag-bound JF₆₆₉ to Ca²⁺-induced conformational changes in the protein (Fig. 1d and Extended Data Fig. 1). We explored different topologies of peptide calmodulin (CaM) insertions into HaloTag^{G171W} at positions spatially proximal to the bound dye and screened for insertions that retained a high dye-ligand-capture rate close to that of HaloTag7 (above 10⁶ M⁻¹s⁻¹)¹⁷ to ensure good labeling with dye-ligand following bolus loading into complex tissue. Insertion of the myosin light-chain kinase (MLCK) CaM-binding peptide followed by CaM at position R179 of HaloTag7^{G171W} resulted in a protein with a fast dye-ligand-capture rate and a modest Ca²⁺-dependent change in fluorescence (Extended Data Figs. 2 and 3). We then performed three rounds of directed evolution on this scaffold with single- and double-site saturation mutagenesis at positions close to the insertion site and the dye–protein interface (Fig. 1e and Extended Data Fig. 4). In total, we screened ~2,000 variants in bacterial lysates and validated ten variants in primary rat hippocampal neuronal culture. We named the variant with the best performance WHaloCaMP1a: it has the fastest dye-ligand-capture rate, the largest

change in fluorescence intensity on addition of Ca²⁺, reasonable Ca²⁺ kinetics (Supplementary Fig. 2), a low one-photon bleaching rate in the absence of Ca²⁺ (Supplementary Fig. 3) and the best performance in neuronal culture. We chose the name WHaloCaMP because the one-letter abbreviation for tryptophan is W, HaloTag is used to localize the dye-ligand to the protein sensor (Halo) and it is a Ca²⁺-modulated protein (CaMP).

WHaloCaMP1a₆₆₉ showed a small increase in absorbance (1.4×) upon binding Ca²⁺ but a larger increase in fluorescence quantum yield (6.2×), which produced an overall Ca²⁺-induced fluorescence emission increase of 7× at 690 nm (Fig. 1f and Table 1). WHaloCaMP1a₆₆₉ is more than twice as bright as jGCaMP8s¹⁸ and 40× brighter than the brightest biliverdin-based near-infrared Ca²⁺ indicator reported to date, iGECI⁷ (Supplementary Table 2), in the Ca²⁺-bound state and shows favorable maximum fluorescence change, Ca²⁺ affinity and kinetics of fluorescence change. WHaloCaMP1a exhibits increased fluorescence emission upon addition of Ca²⁺, making it a ‘positive-going’ indicator, while iGECI and most biliverdin-binding Ca²⁺ indicators show decreased fluorescence upon addition of Ca²⁺.

WHaloCaMP proved to be amenable to further modification of its properties based on previous GECI engineering efforts. We decreased the Ca²⁺ affinity by single point mutations in the MLCK CaM-binding peptide¹⁹ (Extended Data Fig. 5) and produced faster response kinetics by substituting the CaM-binding peptide with endothelial nitric oxide synthase peptide (ENOSP), previously used in the jGCaMP8 series¹⁸ (Extended Data Fig. 6). We also explored other topologies of WHaloCaMP. Several protein engineering efforts^{20,21} have focused on a loop close to the dye-binding site at position T155 of HaloTag7. We generated WHaloCaMP1b by inserting MLCK CaM at position T154 and mutating A151 to tryptophan (Extended Data Fig. 7). We further characterized WHaloCaMP1a in this work because it showed larger fluorescence changes, but we note that the WHaloCaMP1b topology also appears to be a reasonable solution to generating chemogenetic indicators.

A benefit of chemogenetic indicators is that the color of fluorescence emission of the indicator can be altered by changing the small-molecule dye-ligand. In addition to the near-infrared-emitting JF₆₆₉-HaloTag ligand, we explored WHaloCaMP1a bound to other rhodamine-based dyes, including the green-emitting JF₄₉₄-HaloTag ligand, based on 2,7-difluororhodamine 110 (ref. 22), the orange-emitting JF₅₅₂-HaloTag ligand¹³ and the near-infrared-emitting JF₇₂₂-HaloTag ligand¹¹ (Fig. 1g, Extended Data Fig. 8 and Supplementary Figs. 4 and 5). Consistent with a tryptophan PET quenching mechanism, fluorescence changes were mainly conferred by changes in the quantum yield of each bound dye (Table 1). WHaloCaMP1a displayed a high Ca²⁺ affinity (26 ± 2 nM to 71 ± 3 nM for different dyes; Fig. 1g and Table 1), similar to that of jGCaMP8s (46 ± 1 nM)¹⁸. The WHaloCaMP1a sensor bound to different dye-ligands showed Ca²⁺-dependent fluorescence changes from pH 5 to 9. WHaloCaMP1a₆₆₉ was particularly stable, exhibiting little change in Ca²⁺ response in the pH range of 6–8 (Supplementary Fig. 6). The relative pH insensitivity indicates that WHaloCaMP1a could be used in a wide range of cellular compartments.

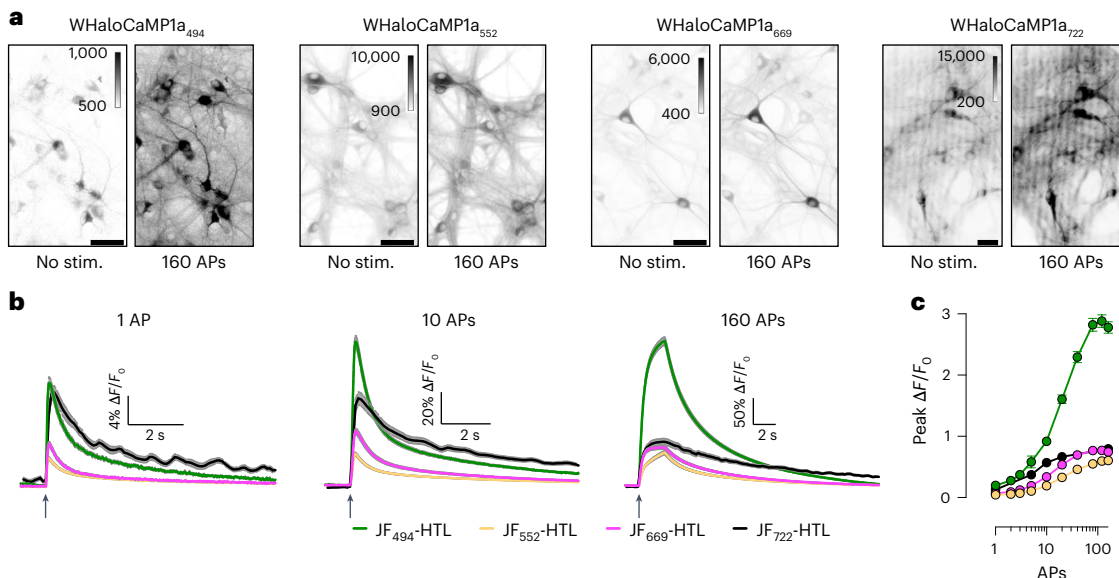


Fig. 2 | Characterization of WHaloCaMP1a in neuronal cultures.

a, Representative images of cultured rat hippocampal neurons expressing WHaloCaMP1a labeled with dye-ligands unstimulated or stimulated with 160 induced APs. Scale bars, 50 μ m. Stim., stimulation. **b**, The $\Delta F/F_0$ response of WHaloCaMP1a expressed in cultured rat hippocampal neurons and labeled with the indicated dye-ligands to trains of APs. Solid line (mean) and gray outline (s.e.m.) for $n = 153, 168$ and 141 neurons for the JF₄₉₄-HaloTag ligand, the

JF₅₅₂-HaloTag ligand and the JF₆₆₉-HaloTag ligand and for $n = 20$ for the JF₇₂₂-HaloTag ligand. Black arrows indicate the start of stimulation. **c**, Peak $\Delta F/F_0$ as a function of the number of APs. Data are presented as mean and s.e.m. for $n = 153, 168$ and 141 neurons for the JF₄₉₄-HaloTag ligand, the JF₅₅₂-HaloTag ligand and the JF₆₆₉-HaloTag ligand and for $n = 20$ for the JF₇₂₂-HaloTag ligand. APs were elicited with a field stimulation electrode with a pulse width of 1 ms at 80 Hz and 40 V.

WHaloCaMP performance in neuron cultures and brain slices

We expressed WHaloCaMP1a in primary rat hippocampal neurons in culture, labeled with dye-ligands and elicited action potentials (APs) evoked by electrical stimulation with a field electrode (Fig. 2a, Supplementary Fig. 7 and Supplementary Tables 3 and 4). WHaloCaMP1a could detect single APs with a $\Delta F/F_0$ value of up to 20% for WHaloCaMP₄₉₄ (Fig. 2b). WHaloCaMP₇₂₂ is the furthest red-shifted chemogenetic fluorescent indicator that can follow single-AP transients in neurons reported to date. In our hands, WHaloCaMP1a₆₆₉ showed a larger max $\Delta F/F_0$ value in neurons than the brightest biliverdin-binding Ca^{2+} indicator, iGECI (Fig. 2c and Supplementary Tables 3 and 4). In addition, WHaloCaMP1a₆₆₉ showed faster time to peak and half decay time than iGECI (Supplementary Figs. 7 and 8), making it better suited to capture neuronal activity.

The excitation spectrum of WHaloCaMP1a₆₆₉ is better separated from the action spectrum of many blue-excited optogenetic tools than that of red Ca^{2+} indicators. We found via electrophysiology that the light required for exciting WHaloCaMP1a₆₆₉ did not produce any observable membrane depolarization in neurons expressing the sensitive channelrhodopsin variant CheRiff²³ (Supplementary Fig. 9). Indeed, even at a light intensity exceeding ten times the power required for functional imaging with WHaloCaMP1a₆₆₉, no depolarization was observed. By contrast, the light required for imaging the commonly used red fluorescent protein-based Ca^{2+} indicator jRCaMP1a produced substantial subthreshold depolarization of neurons expressing CheRiff.

The near-infrared emission of WHaloCaMP1a₆₆₉ also allows for multiplexing with current fluorescent protein-based indicators. We performed simultaneous multiplexed two-photon imaging of fluctuating Ca^{2+} and protein kinase A (PKA) activity in response to muscarinic acetylcholine receptor (mAChR) and adenylate cyclase activation in acute mouse brain slices using WHaloCaMP1a₆₆₉ and a green PKA activity indicator, FLIM-AKAR²⁴ (Supplementary Fig. 10). Consistent with previous results with single-reporter imaging^{25,26}, we observed a concurrent Ca^{2+} and PKA activity increase in response to mAChR activation and only increased PKA phosphorylation in response to adenylate

cyclase activation. Because a Ca^{2+} increase is upstream of PKA activation, these results demonstrate the possibility of tracking concurrent dynamics of multiple signals to understand temporal transformations in a signaling transduction cascade.

WHaloCaMP1a reports neuronal Ca^{2+} in flies and mice

Because previous chemogenetic HaloTag-based sensors, such as HaloCaMPs, were limited to experiments in reduced preparations, we explored whether WHaloCaMP1a could be expressed, labeled with dye-ligands and used to follow physiological Ca^{2+} responses in living animals. Although WHaloCaMP1a₇₂₂ showed large responses in primary cultured neurons (Fig. 2), the JF₇₂₂-HaloTag ligand did not appear to be bioavailable in vivo (Supplementary Note 1). Instead, we focused on the dyes that showed the best in vivo bioavailability: the JF₅₅₂-HaloTag ligand and the JF₆₆₉-HaloTag ligand. First, we tested whether WHaloCaMP1a could report odor-evoked Ca^{2+} responses in mushroom body Kenyon cells (KCs) in adult *Drosophila* (Fig. 3a). KCs are third-order neurons in the fly olfactory pathway, and their odor response profile has been extensively characterized²⁷. We expressed WHaloCaMP1a in KCs with the mushroom body driver R13F02-Gal4. We then opened a small window in the head capsule of flies to expose the calyx, which houses the dendritic processes of all KCs (Fig. 3b), and labeled WHaloCaMP1a with JF₆₆₉-HaloTag ligand by application in saline solution. Upon odor presentation, we observed clear WHaloCaMP1a₆₆₉ fluorescence increases in individual trials in response to apple cider vinegar as well as two chemical odors (Fig. 3b and Supplementary Fig. 11). Similar responses were observed when we labeled WHaloCaMP with the JF₅₅₂-HaloTag ligand, highlighting the spectral flexibility of the indicator. Trends in odor response were similar to that of the red fluorescent protein-based Ca^{2+} indicator jRGECO1a²⁸ (Supplementary Fig. 12).

We then tested the performance of WHaloCaMP1a in mice. We expressed WHaloCaMP1a with an enhanced green fluorescent protein (EGFP) expression marker from the Ca^{2+} -CaM-dependent protein kinase II (CaMKII) promoter in the mouse primary visual cortex (V1) using adeno-associated virus (AAV)-mediated gene delivery (Fig. 3c).

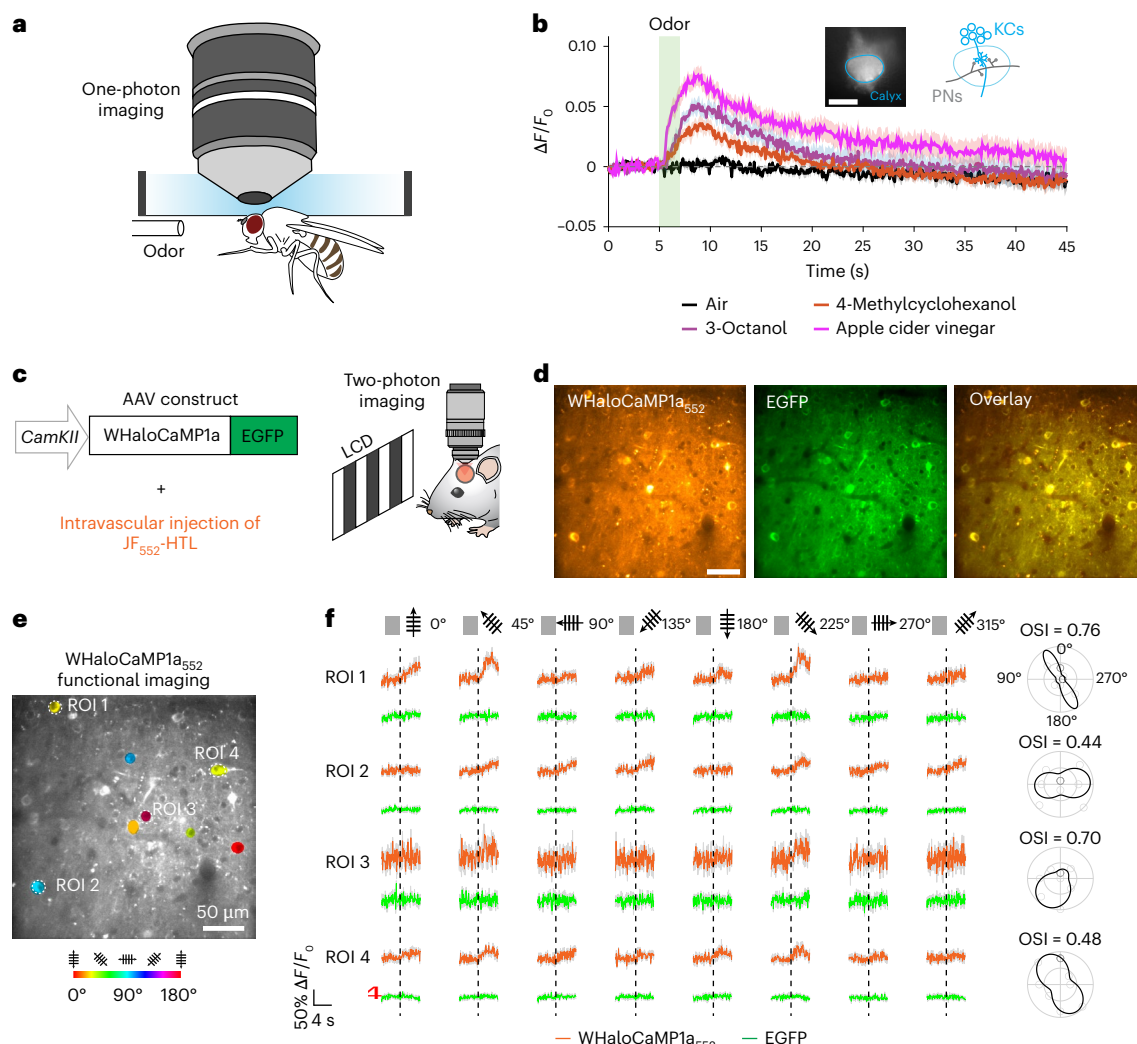


Fig. 3 | WHaloCaMP1a reports on neuronal activity in flies and mice. **a**, One-photon imaging setup of head-fixed flies expressing WHaloCaMP1a labeled with dye-ligands. **b**, Fluorescence responses from WHaloCaMP1a₆₆₉ in head-fixed flies presented with different odors. WHaloCaMP1a was expressed in mushroom body KCs. Images were acquired from the calyx, where KCs receive dendritic inputs from the olfactory projection neurons (PNs) (insets). Green shading indicates odor presentation for 2 s. Data were from six flies, and odors were presented three times to each fly. The thick line and the shaded areas indicate means and s.e.m. across odor trials. Scale bar, 50 μ m. **c**, AAV construct for transducing neurons in the mouse V1 and the schematic of the experimental setup for two-photon functional imaging of WHaloCaMP1a in the visual cortex of mice. The JF₅₅₂-HaloTag ligand was intravascularly injected 1 d before examining orientation.

selectivity of V1 neurons in the anesthetized mouse exposed to moving grafted visual stimuli of different orientations and directions. LCD, liquid crystal display. **d**, Representative images of a field of view in the mouse V1 showing neurons expressing WHaloCaMP1a₅₅₂ or EGFP. Scale bar, 50 μ m. **e**, Functional imaging of V1 neurons shows the orientation selectivity map. **f**, Functional imaging of $\Delta F/F_0$ (WHaloCaMP1a₅₅₂ channel) or control (EGFP channel) traces (ROI1–4) in response to drifting gratings in the directions shown above the traces. Average of five trials. Colored lines indicate means, and shadows indicate s.d. Orientation selectivity index (OSI) of cells is shown on the right. Imaging rate was 15 Hz. A representative imaging session from three imaging sessions is shown. The experiment was repeated independently 19 times in four mice with similar results.

Intravenous delivery of the JF₅₅₂-HaloTag ligand or the JF₆₆₉-HaloTag ligand via retro-orbital (r.o.) injection successfully labeled WHaloCaMP1a expressed in V1 excitatory neurons (Fig. 3d and Supplementary Figs. 13 and 14). We observed clear visually evoked Ca^{2+} transients in layer 2/3 excitatory neurons with WHaloCaMP1a₆₆₉ using 1,225-nm two-photon excitation in single trials (Supplementary Fig. 13). As most standard two-photon microscopes cannot achieve substantial 1,225-nm excitation, we instead labeled WHaloCaMP1a with the JF₅₅₂-HaloTag ligand and imaged at either 850 nm or 1,050 nm. Using 850-nm light, we could co-excite the EGFP expression marker and cleanly separate the fluorescence emission, providing a nonresponsive normalization channel during two-photon functional imaging, while 1,050-nm light selectively excited WHaloCaMP1a₅₅₂ (Supplementary Fig. 14). We performed functional imaging during presentation of drifting grating

visual stimuli to the mouse's contralateral eye and observed responses in individual trials up to 35% $\Delta F/F_0$ as well as orientation tuning of the responses, which is a hallmark of V1 excitatory neurons (Fig. 3e,f and Supplementary Figs. 15 and 16).

When we expressed WHaloCaMP1a₆₆₉-EGFP or iGECI-EGFP in the S1 somatosensory barrel cortex, we observed higher expression and maximum far-red fluorescence signal from WHaloCaMP1a₆₆₉ when imaged by one-photon microscopy (Supplementary Fig. 17). Additionally, we could observe clear functional responses of WHaloCaMP1a₆₆₉ elicited by whisker stimulation of the mouse.

Functional imaging in zebrafish larvae with WHaloCaMP1a₆₆₉. We generated transgenic zebrafish expressing WHaloCaMP1a under the pan-neuronal *elavl3* promoter. First, we verified that we could perform

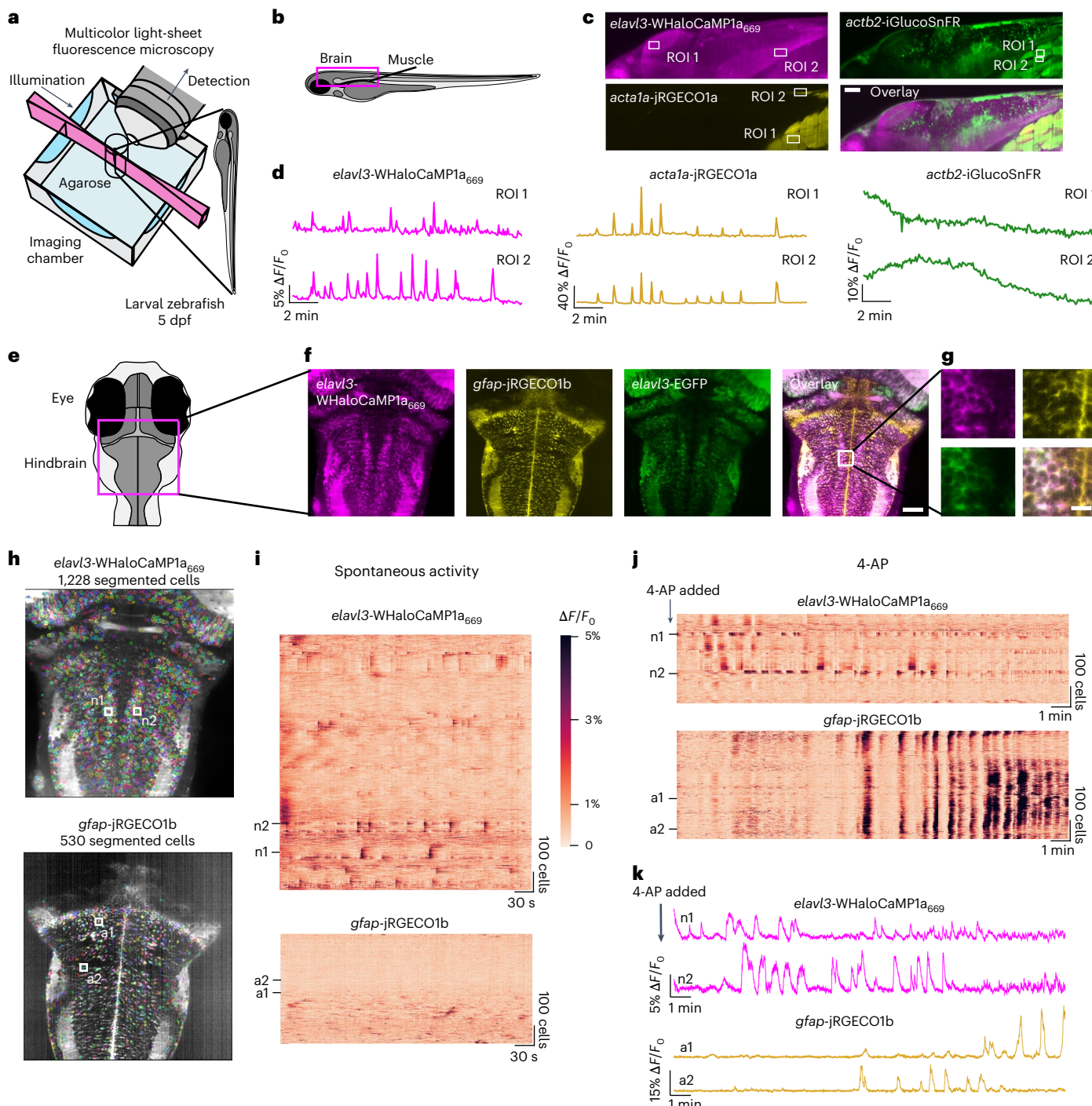


Fig. 4 | Three-color multiplexed functional imaging in zebrafish larvae.

a, Light-sheet imaging setup for multiplexed imaging. **b**, Schematic of side-view zebrafish larvae highlighting the field of view for three-color multiplexed functional imaging of glucose and Ca^{2+} in muscles and neurons. **c**, Representative images of WHaloCaMP1a expressed in neurons from the *elav3* promoter, iGlucoSnFR expressed from the *actb2* ubiquitous promoter and jRGECO1a expressed in muscle from the *acta1a* promoter. Scale bar, 50 μm . The experiment was repeated independently three times with similar results. **d**, Fluorescence $\Delta F/F_0$ traces of WHaloCaMP1a₆₆₉, jRGECO1a and iGlucoSnFR in the ROI outlined in **b**. A representative experiment from three zebrafish larvae was imaged. **e**, Schematic of the zebrafish larva's head indicating the field of view for light-sheet imaging of neuronal and astrocyte activity. **f**, Representative images of the expression patterns of WHaloCaMP1a₆₆₉-EGFP expressed under the *elav3*

promoter and jRGECO1b expressed under the *gfap* promoter. Scale bar, 50 μm . The experiment was repeated independently more than three times with similar results. **g**, Zoomed-in images showing single-cell resolution of fluorescent signals in the hindbrain. Scale bar, 20 μm . **h**, Images of Suite2p- and Cellpose-segmented cells from simultaneous functional imaging of WHaloCaMP1a₆₆₉ and jRGECO1b. **i**, Rastermaps of activity from 1,228 segmented neurons (top) and 530 astrocytes (bottom) during spontaneous brain activity. Two neurons (n1 and n2) indicate the hindbrain oscillator. Two astrocytes (a1 and a1) are also indicated. **j**, The compound 4-AP was added to the imaging chamber of the zebrafish larva imaged in **i**, and functional imaging was performed. Concatenation of three imaging blocks of 6.2 min each. **k**, Fluorescence $\Delta F/F_0$ traces of n1 and n2 (top) and a1 and a2 (bottom) after addition of 4-AP.

whole-brain functional neuronal imaging with larvae at 4–5 d post fertilization (dpf) with WHaloCaMP1a₆₆₉ using light-sheet imaging with excitation at 685 nm and 4 Hz (Extended Data Fig. 9 and Supplementary Video 1). To benchmark the performance of WHaloCaMP1a₆₆₉ against known red Ca²⁺ indicators²⁸, we crossed the *elavl3*-WHaloCaMP1a zebrafish line with a line expressing pan-neuronal red fluorescent protein-based calcium indicator jRGECO1b under the same *elavl3* promoter. We performed dual-color light-sheet imaging (excitation at 561 nm and 640 nm) from a single plane in the hindbrain of zebrafish larvae at 4–5 dpf. WHaloCaMP1a₆₆₉ reported all the Ca²⁺ transients observed with jRGECO1b in a region of interest (ROI) in the hindbrain, albeit with lower maximum $\Delta F/F_0$ than the jRGECO1b signal (66% of the maximum $\Delta F/F_0$ signal of jRGECO1b; Supplementary Fig. 18).

Multiplexed imaging in zebrafish larvae with WHaloCaMP1a₆₆₉
 Clean spectral separation of WHaloCaMP1a₆₆₉ from green and red fluorescent proteins enabled us to perform three-color multiplexed imaging in zebrafish larvae (Fig. 4a). To simultaneously follow three physiological signals, we crossed the transgenic line expressing pan-neuronal WHaloCaMP1a with a previously established line²⁹ expressing the green-emitting glucose sensor iGlucoSnFR throughout the body of the fish using the β -actin promoter and the red-emitting Ca²⁺ indicator jRGECO1a in skeletal muscle using the α -actinin promoter. After labeling WHaloCaMP1a with the JF₆₆₉-HaloTag ligand, we performed light-sheet imaging of a single plane in the fish (Fig. 4b) with clear spectral separation of the fluorescence emission of the three sensors (Fig. 4c, Supplementary Fig. 19 and Supplementary Video 2). Ca²⁺ transients in the zebrafish hindbrain neurons recorded using WHaloCaMP1a₆₆₉ correlated with Ca²⁺ transients in skeletal muscle recorded using jRGECO1a, but neuronal signals in other parts of the brain, such as the optical tectum, did not (Fig. 4d). Glucose changes in muscle observed using iGlucoSnFR were substantially slower than either the neuronal or muscle Ca²⁺ transients, as previously reported²⁹.

Next, we asked whether WHaloCaMP could be used to follow changes in neuronal activity to report changes in physiological states during multiplexed imaging. The activities of neurons and radial astrocytes are both linked to changes in behavior³⁰, as reported by dual-color functional imaging. We imaged zebrafish larvae expressing WHaloCaMP1a₆₆₉ in neurons and the red Ca²⁺ indicator jRGECO1b in radial astrocytes, thus freeing up the green fluorescence emission channel, here using it as a fluorescent marker for neurons (Fig. 4e,f). Using light-sheet imaging, we could clearly resolve single cells in a plane of the zebrafish hindbrain (Fig. 4g). We then performed functional imaging of paralyzed zebrafish larvae at 4 Hz and used Suite2p³¹ together with Cellpose³² and Rastermap³³ (Fig. 4h and Supplementary Fig. 20) to segment and follow the activity of over 1,000 neurons and hundreds of astrocytes simultaneously during spontaneous activity (Fig. 4i and Supplementary Video 3). Without any external perturbation, WHaloCaMP1a₆₆₉ clearly showed Ca²⁺ transients in a population of neurons that form part of the hindbrain oscillator³⁴ related to motor control during swimming (n1 and n2 in Fig. 4i). Leading up to and during seizure-like states, induced by the potassium channel blocker 4-aminopyridine (4-AP), the pattern of neuronal activity in the hindbrain oscillator was lost (n1 and n2 in Fig. 4j,k and Supplementary Video 4), which has previously been described to be due to hyperexcitability³⁵ of the neurons. We also observed large Ca²⁺ waves in the astrocyte population in response to 4-AP (a1 and a2 in Fig. 4j,k), as previously described³⁶, which we could clearly separate from the neuronal activity, as the emissions of jRGECO1b and WHaloCaMP1a₆₆₉ are 100 nm apart. The loss of hindbrain oscillator activity and the large astrocytic Ca²⁺ waves were not observed in fish not treated with 4-AP (Supplementary Fig. 21). WHaloCaMP1a₆₆₉ is well suited for one-photon multicolor experiments in living animals as it can be excited with common far-red and near-infrared laser lines, and the emission is separated from commonly used fluorescent proteins.

FLIM using WHaloCaMP1a

The fluorescence modulation in WHaloCaMP1a on binding to Ca²⁺ is mainly due to changes in quantum yield. We thus explored WHaloCaMP1a as a FLIM probe for Ca²⁺ (Fig. 5a). Fluorescence lifetime is an inherent property of fluorophores, and FLIM allows absolute concentrations to be determined using fluorescent biosensors, which allows comparison of analytes across imaging days, samples and animals³⁷. FLIM imaging has been used to determine how Ca²⁺ concentrations differ in astrocytes and neurons during development³⁸ and during affinity maturation of B cells in living mice³⁹. However, the technique is limited by the number of photons that can be collected for accurate fitting of fluorescent lifetimes.

WHaloCaMP1a bound to JF₄₉₄, JF₅₅₂, JF₆₆₉ and JF₇₂₂ could all be used as FLIM probes for Ca²⁺ (Extended Data Fig. 10). As WHaloCaMP1a₆₆₉ is brightly fluorescent, we reasoned that it would perform especially well as a FLIM probe in living cells and animals. In purified protein solutions, we observed a 2.1-ns increase in the fluorescence lifetime of WHaloCaMP1a₆₆₉ upon Ca²⁺ binding (lifetime of calcium-free τ_{apo} = 1.3 ns versus lifetime of calcium-saturated τ_{sat} = 3.4 ns) (Fig. 5b). We then generated calibration curves of lifetime versus Ca²⁺ concentration both with purified protein and with HeLa cells expressing WHaloCaMP1a₆₆₉ that were permeabilized by digitonin (Fig. 5c and Supplementary Fig. 22). We used these calibration curves to follow Ca²⁺ dynamics in HeLa cells stimulated with histamine (Fig. 5d, Supplementary Fig. 23 and Supplementary Video 5). As the Ca²⁺ affinity of WHaloCaMP1a₆₆₉ is higher than that of the previously reported turquoise-emitting FLIM Ca²⁺ indicator Tq-Ca-FLITS⁴⁰, we could more accurately determine low Ca²⁺ concentrations, down to 7 nM (Fig. 5e). We measured over 100-fold changes in Ca²⁺ concentration during histamine-induced oscillations in HeLa cells. To determine whether WHaloCaMP allowed *in vivo* FLIM Ca²⁺ imaging, zebrafish larvae expressing WHaloCaMP1a were labeled with JF₆₆₉-HaloTag ligand and imaged with a commercial confocal FLIM microscope (Fig. 5f and Supplementary Fig. 24). We could follow dynamic changes in absolute intracellular Ca²⁺ concentration in populations of forebrain neurons at single-cell resolution during spontaneous activity at one frame per second (Fig. 5g and Supplementary Video 6), and Ca²⁺ events seen by FLIM matched well with those observed via fluorescence intensity changes. WHaloCaMP therefore allows for the quantitative readout of physiological signaling at cellular resolution across tissues *in vivo*.

Discussion

Despite their favorable photophysical properties, synthetic dyes have not been fully exploited to build chemogenetic functional indicators with applications in living animals, especially in the near-infrared. This has mostly been due to challenges with delivering the dyes in complex tissue and *in vivo*. Here, we started with a near-infrared dye-ligand, JF₆₆₉-HaloTag ligand, which we knew could be delivered to many tissues in mice after vascular injection, and built a Ca²⁺ indicator around it. Because the JF₆₆₉-HaloTag ligand did not work with our existing chemogenetic indicators, we used a different mechanism to modulate its fluorescence output: PET quenching by a strategically placed tryptophan. This strategy allowed us to record Ca²⁺ transients in the near-infrared channel *in vivo* in several model organisms.

The chemogenetic approach leads to several advantageous properties of WHaloCaMP compared to biliverdin-binding protein-based indicators. WHaloCaMP1a₆₆₉ is up to 40× brighter than biliverdin-binding indicators. For some applications, the endogenous availability of biliverdin cofactor in cells is advantageous, as supplementation of the exogenous cofactor is not required^{6,7}. However, the affinity for biliverdin is often weak in the Ca²⁺ indicators built from biliverdin-binding proteins, making them dim when used in animals. As opposed to the JF₆₆₉-HaloTag ligand, biliverdin does not cross the blood–brain barrier in mice; therefore, additional biliverdin must be generated *in situ* by either delivery of additional biliverdin-producing enzymes⁴¹ or

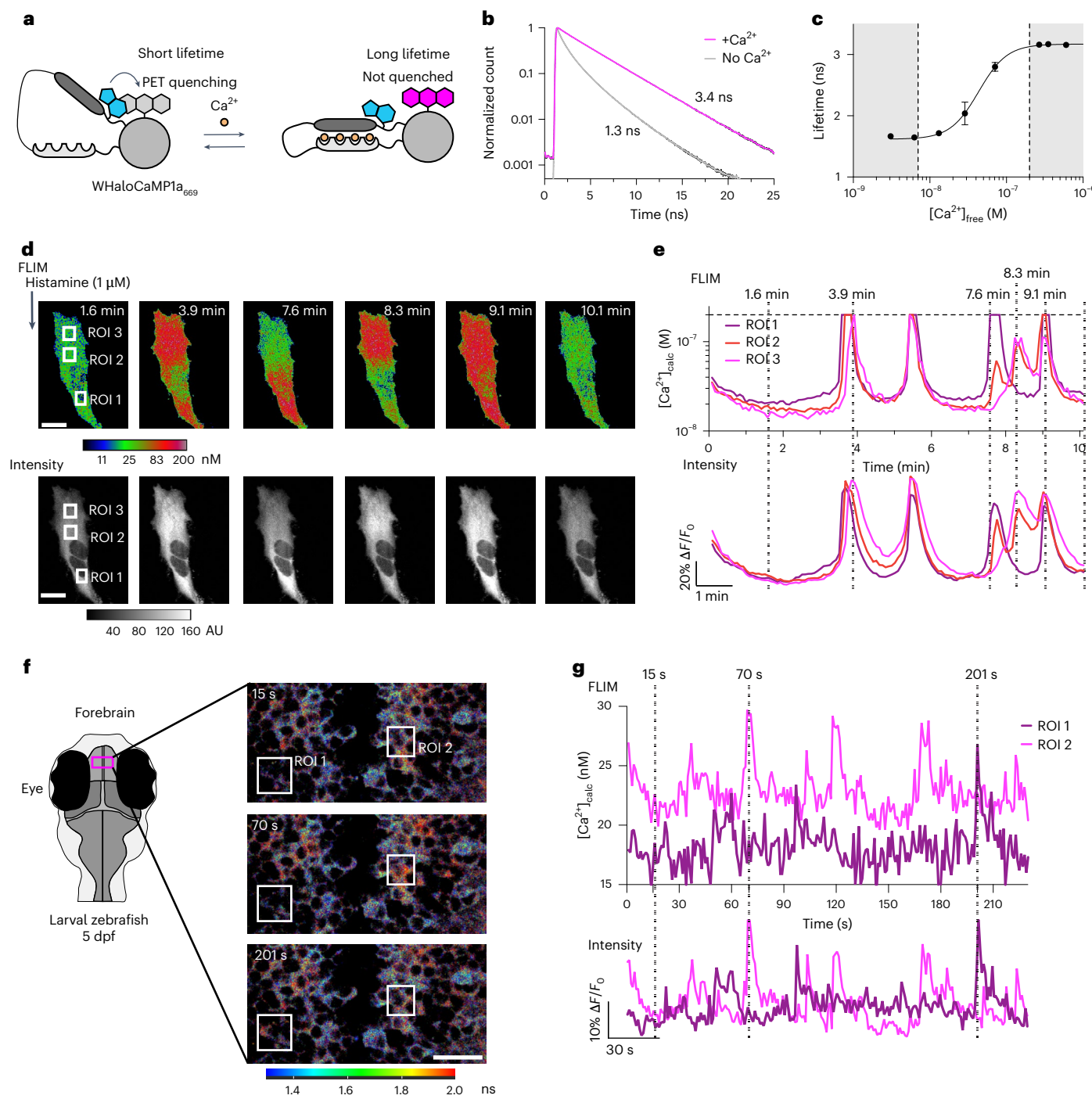


Fig. 5 | Quantitative Ca²⁺ measurements by FLIM using WHaloCaMP1a. **a**, Schematic of WHaloCaMP1a bound to a dye-ligand used as a FLIM probe. Tryptophan quenching modulates the fluorescence lifetime. **b**, Normalized fluorescence lifetime of WHaloCaMP1a₆₆₉ in the presence or the absence of Ca²⁺, fit to a three-component fluorescence decay. **c**, Calibration curve of the averaged fluorescence lifetime of WHaloCaMP1a₆₆₉ versus Ca²⁺ concentration. The white box indicates the range in which WHaloCaMP1a₆₆₉ can be used to make quantitative measurements of Ca²⁺ concentration. Performed with purified protein. Mean of three replicates and s.d. are plotted. **d**, Pseudocolored concentration (top) and intensity images (bottom) of WHaloCaMP1a₆₆₉ in HeLa cells after histamine addition. Scale bar, 20 μm. Color bar indicates Ca²⁺ concentration, calculated from a calibration curve of fluorescence lifetime. AU, arbitrary units. **e**, Quantitative Ca²⁺ concentration calculated (calc) from a FLIM calibration curve (top) and fluorescence traces $\Delta F/F_0$ calculated from the intensity channel (bottom) in histamine-stimulated HeLa cells in the ROI highlighted in **d**. Calibrated WHaloCaMP1a₆₆₉ can only be used to measure Ca²⁺ concentrations up to 200 nM, indicated by a dashed horizontal line. Vertical dashed lines indicate time points in the time series at which images in **d** are shown. **f**, FLIM of WHaloCaMP1a₆₆₉ in live zebrafish larvae showing spontaneous neuronal activity in the forebrain. The experiment was repeated independently three times with similar results. Schematic indicating the field of view during imaging (left). Overlaid images of FLIM and intensity using Leica LAS X software, with a color bar indicating the fluorescence lifetime. Scale bar, 20 μm. **g**, Ca²⁺ concentrations calculated from a FLIM calibration curve (top) and fluorescence traces $\Delta F/F_0$ calculated from the intensity channel (bottom) over time for two neurons in the forebrain of zebrafish larvae from the ROI indicated in **f**. Dashed lines indicate time points of images in **f**. Representative images from three imaging sessions.

the intensity channel (bottom) in histamine-stimulated HeLa cells in the ROI highlighted in **d**. Calibrated WHaloCaMP1a₆₆₉ can only be used to measure Ca²⁺ concentrations up to 200 nM, indicated by a dashed horizontal line. Vertical dashed lines indicate time points in the time series at which images in **d** are shown. **f**, FLIM of WHaloCaMP1a₆₆₉ in live zebrafish larvae showing spontaneous neuronal activity in the forebrain. The experiment was repeated independently three times with similar results. Schematic indicating the field of view during imaging (left). Overlaid images of FLIM and intensity using Leica LAS X software, with a color bar indicating the fluorescence lifetime. Scale bar, 20 μm. **g**, Ca²⁺ concentrations calculated from a FLIM calibration curve (top) and fluorescence traces $\Delta F/F_0$ calculated from the intensity channel (bottom) over time for two neurons in the forebrain of zebrafish larvae from the ROI indicated in **f**. Dashed lines indicate time points of images in **f**. Representative images from three imaging sessions.

knockouts of biliverdin-consuming proteins⁴². A further advantage of WHaloCaMP's chemigenetic nature over fixed chromophore systems is that the color of the fluorescence emission can be tuned depending on the experimental requirements. Here, we show that the same genetically encoded protein sensor, WHaloCaMP1a, can be used with a range of rhodamine dye-ligands with green to near-infrared emission for functional imaging. WHaloCaMP1a thus allows flexibility to match the excitation and emission requirements for specific imaging hardware or for spectrally multiplexed functional imaging.

WHaloCaMP was amenable to known protein engineering strategies to alter Ca²⁺ affinity and binding kinetics, and we envision further protein engineering to optimize maximum fluorescence change. Given the breadth of existing fluorescent protein⁴³ and HaloTag or dye-based functional indicators¹⁴, we anticipate that the tryptophan-quenching chemigenetic indicator approach can be extended to *in vivo* imaging of other physiological signals. Additionally, as we learn more about the bioavailability of dye-ligands in animals, we envision additional chemigenetic approaches in which the specificity of genetically encoded tools is combined with the brightness, the photostability and the tunability of synthetic dyes.

Online content

Any methods, additional references, Nature Portfolio reporting summaries, source data, extended data, supplementary information, acknowledgements, peer review information; details of author contributions and competing interests; and statements of data and code availability are available at <https://doi.org/10.1038/s41592-024-02411-6>.

References

1. Kim, T. H. & Schnitzer, M. J. Fluorescence imaging of large-scale neural ensemble dynamics. *Cell* **185**, 9–41 (2022).
2. O'Banion, C. P. & Yasuda, R. Fluorescent sensors for neuronal signaling. *Curr. Opin. Neurobiol.* **63**, 31–41 (2020).
3. Sabatini, B. L. & Tian, L. Imaging neurotransmitter and neuromodulator dynamics *in vivo* with genetically encoded indicators. *Neuron* **108**, 17–32 (2020).
4. Liu, P., Mu, X., Zhang, X.-D. & Ming, D. The near-infrared-II fluorophores and advanced microscopy technologies development and application in bioimaging. *Bioconjug. Chem.* **31**, 260–275 (2020).
5. Farrants, H. & Tebo, A. G. Fluorescent chemigenetic actuators and indicators for use in living animals. *Curr. Opin. Pharmacol.* **62**, 159–167 (2022).
6. Qian, Y. et al. A genetically encoded near-infrared fluorescent calcium ion indicator. *Nat. Methods* **16**, 171–174 (2019).
7. Shemetov, A. A. et al. A near-infrared genetically encoded calcium indicator for *in vivo* imaging. *Nat. Biotechnol.* **39**, 368–377 (2021).
8. Gautier, A. & Tebo, A. G. Sensing cellular biochemistry with fluorescent chemical–genetic hybrids. *Curr. Opin. Chem. Biol.* **57**, 58–64 (2020).
9. Deo, C. et al. The HaloTag as a general scaffold for far-red tunable chemigenetic indicators. *Nat. Chem. Biol.* **17**, 718–723 (2021).
10. Grimm, J. B. et al. A general method to fine-tune fluorophores for live-cell and *in vivo* imaging. *Nat. Methods* **14**, 987–994 (2017).
11. Grimm, J. B. et al. A general method to optimize and functionalize red-shifted rhodamine dyes. *Nat. Methods* **17**, 815–821 (2020).
12. Mohar, B. et al. Brain-wide measurement of protein turnover with high spatial and temporal resolution. Preprint at *bioRxiv* <https://doi.org/10.1101/2022.11.12.516226> (2022).
13. Zheng, Q. et al. Rational design of fluorogenic and spontaneously blinking labels for super-resolution imaging. *ACS Cent. Sci.* **5**, 1602–1613 (2019).
14. Frei, M. S. et al. Engineered HaloTag variants for fluorescence lifetime multiplexing. *Nat. Methods* **19**, 65–70 (2022).
15. Hellweg, L. et al. A general method for the development of multicolor biosensors with large dynamic ranges. *Nat. Chem. Biol.* **19**, 1147–1157 (2023).
16. Vaiana, A. C. et al. Fluorescence quenching of dyes by tryptophan: interactions at atomic detail from combination of experiment and computer simulation. *J. Am. Chem. Soc.* **125**, 14564–14572 (2003).
17. Wilhelm, J. et al. Kinetic and structural characterization of the self-labeling protein tags HaloTag7, SNAP-tag, and CLIP-tag. *Biochemistry* **60**, 2560–2575 (2021).
18. Zhang, Y. et al. Fast and sensitive GCaMP calcium indicators for imaging neural populations. *Nature* **615**, 884–891 (2023).
19. Fosque, B. F. et al. Labeling of active neural circuits *in vivo* with designed calcium integrators. *Science* **347**, 755–760 (2015).
20. Ishikawa, H., Meng, F., Kondo, N., Iwamoto, A. & Matsuda, Z. Generation of a dual-functional split-reporter protein for monitoring membrane fusion using self-associating split GFP. *Protein Eng. Des. Sel.* **25**, 813–820 (2012).
21. Hiblot, J. et al. Luciferases with tunable emission wavelengths. *Angew. Chem. Int. Ed.* **56**, 14556–14560 (2017).
22. Grimm, J. B. & Lavis, L. D. Synthesis of rhodamines from fluoresceins using Pd-catalyzed C–N cross-coupling. *Org. Lett.* **13**, 6354–6357 (2011).
23. Hochbaum, D. R. et al. All-optical electrophysiology in mammalian neurons using engineered microbial rhodopsins. *Nat. Methods* **11**, 825–833 (2014).
24. Chen, Y., Saulnier, J., Yellen, G. & Sabatini, B. A PKA activity sensor for quantitative analysis of endogenous GPCR signaling via 2-photon FRET–FLIM imaging. *Front. Pharmacol.* **5**, 56 (2014).
25. Chen, Y. et al. Endogenous Gaq-coupled neuromodulator receptors activate protein kinase A. *Neuron* **96**, 1070–1083 (2017).
26. Tilden, E. I., Maduskar, A., Oldenborg, A., Sabatini, B. L. & Chen, Y. A Cre-dependent reporter mouse for quantitative real-time imaging of protein kinase A activity dynamics. *Sci. Rep.* **14**, 3054 (2024).
27. Honegger, K. S., Campbell, R. A. A. & Turner, G. C. Cellular-resolution population imaging reveals robust sparse coding in the *Drosophila* mushroom body. *J. Neurosci.* **31**, 11772–11785 (2011).
28. Dana, H. et al. Sensitive red protein calcium indicators for imaging neural activity. *eLife* **5**, e12727 (2016).
29. Keller, J. P. et al. *In vivo* glucose imaging in multiple model organisms with an engineered single-wavelength sensor. *Cell Rep.* **35**, 109284 (2021).
30. Mu, Y. et al. Glia accumulate evidence that actions are futile and suppress unsuccessful behavior. *Cell* **178**, 27–43 (2019).
31. Pachitariu, M. et al. Suite2p: beyond 10,000 neurons with standard two-photon microscopy. Preprint at *bioRxiv* <https://doi.org/10.1101/061507> (2017).
32. Stringer, C., Wang, T., Michaelos, M. & Pachitariu, M. Cellpose: a generalist algorithm for cellular segmentation. *Nat. Methods* **18**, 100–106 (2021).
33. Stringer, C. et al. Rastermap: a discovery method for neural population recordings. Preprint at *bioRxiv* <https://doi.org/10.1101/2023.07.25.550571> (2023).
34. Ahrens, M. B., Orger, M. B., Robson, D. N., Li, J. M. & Keller, P. J. Whole-brain functional imaging at cellular resolution using light-sheet microscopy. *Nat. Methods* **10**, 413–420 (2013).
35. Liu, J. & Baraban, S. C. Network properties revealed during multi-scale calcium imaging of seizure activity in zebrafish. *eNeuro* **6**, ENEURO.0041-0019.2019 (2019).

36. Winter, M. J. et al. 4-Dimensional functional profiling in the convulsant-treated larval zebrafish brain. *Sci. Rep.* **7**, 6581 (2017).
37. Ma, P. et al. Fast and slow: recording neuromodulator dynamics across both transient and chronic time scales. *Sci. Adv.* **10**, eadi0643 (2024).
38. Zheng, K. et al. Time-resolved imaging reveals heterogeneous landscapes of nanomolar Ca^{2+} in neurons and astroglia. *Neuron* **88**, 277–288 (2015).
39. Ulbricht, C. et al. Intravital quantification reveals dynamic calcium concentration changes across B cell differentiation stages. *eLife* **10**, e56020 (2021).
40. van der Linden, F. H. et al. A turquoise fluorescence lifetime-based biosensor for quantitative imaging of intracellular calcium. *Nat. Commun.* **12**, 7159 (2021).
41. Qian, Y. et al. Improved genetically encoded near-infrared fluorescent calcium ion indicators for *in vivo* imaging. *PLoS Biol.* **18**, e3000965 (2020).
42. Kobachi, K. et al. Biliverdin reductase-A deficiency brighten and sensitize biliverdin-binding chromoproteins. *Cell Struct. Funct.* **45**, 131–141 (2020).
43. Wang, M., Da, Y. & Tian, Y. Fluorescent proteins and genetically encoded biosensors. *Chem. Soc. Rev.* **52**, 1189–1214 (2023).
44. Cook, A., Walterspiel, F. & Deo, C. HaloTag-based reporters for fluorescence imaging and biosensing. *ChemBioChem* **24**, e202300022 (2023).

Publisher's note Springer Nature remains neutral with regard to jurisdictional claims in published maps and institutional affiliations.

Open Access This article is licensed under a Creative Commons Attribution 4.0 International License, which permits use, sharing, adaptation, distribution and reproduction in any medium or format, as long as you give appropriate credit to the original author(s) and the source, provide a link to the Creative Commons licence, and indicate if changes were made. The images or other third party material in this article are included in the article's Creative Commons licence, unless indicated otherwise in a credit line to the material. If material is not included in the article's Creative Commons licence and your intended use is not permitted by statutory regulation or exceeds the permitted use, you will need to obtain permission directly from the copyright holder. To view a copy of this licence, visit <http://creativecommons.org/licenses/by/4.0/>.

© The Author(s) 2024

Methods

Molecular biology

Synthetic DNA oligonucleotides were purchased from Twist Bioscience and Integrated DNA Technologies. Q5 High-Fidelity DNA Polymerase (New England Biolabs) was used for all PCR amplifications. Isothermal assembly reactions were performed with a NEBuilder HiFi kit (New England Biolabs). Small-scale DNA isolation was performed with the QIAprep Spin Miniprep Kit (Qiagen). Vector backbones were acquired from the following sources: pRSET was acquired from Life Technologies; pGP-AAV-syn-jGCaMP7f-WPRE was a gift from D. Kim (GENIE project, Janelia Research Campus, Howard Hughes Medical Institute, Ashburn, VA, USA) and the GENIE project (Addgene plasmid 104488); pAAV-CaMKIIa-EGFP was a gift from B. Roth (Department of Pharmacology, University of North Carolina at Chapel Hill School of Medicine, Chapel Hill, NC, USA; Addgene plasmid 50469); p10xUAS-IVS-Syn21-Voltron-p10 was from a previously deposited Addgene plasmid (Addgene plasmid 119041); pTol2-HuC(*elavl3*)-CaMPARI2 was from a previously deposited Addgene plasmid (Addgene plasmid 137185); piGECI-N1 was a gift from V. Verkusha (Department of Genetics, Albert Einstein College of Medicine, Bronx, NY, USA; Addgene plasmid 160421); pBAD-iGECInano was a gift from V. Verkusha (Addgene plasmid 186189). pCAGGS was used from an in-house source. Cloning was conducted by PCR amplification (pDUET, pRSET) or restriction enzyme digestion of vector backbones. For use in mammalian cell culture, inserts were cloned into pCAGGS at the AflIII and AgeI restriction sites. For use in rodent neurons, the inserts were cloned into pAAV-hsyn or pAAV-CaMKII at the BamHI and HindIII restriction sites. For expression in *Danio rerio* pTol2 with the HuC *elavl3* promoter, the inserts were cloned into the AgeI restriction site. For expression in *Drosophila melanogaster*, the insert was cloned into 10XUAS-IVS-Syn21 at the Xhol and XbaI restriction sites.

Inserts were amplified by PCR. WHaloCaMP constructs were cloned with a nuclear exclusion signal (NES) to mimic the cellular localization of jGCaMPs in neurons. Vector backbones and inserts were assembled by isothermal assembly with an overlap of 10–30 bp, and the sequence was verified by Sanger sequencing (Azenita Life Sciences) or by nanopore full-plasmid sequencing (Plasmidsaurus). For large-scale plasmid preparation, DNA was isolated by the Janelia Molecular Biology Facility. AAVs were prepared by Janelia Virus Services. Plasmids generated in this work have been deposited with Addgene: pRSET-WHaloCaMP1a-EGFP (205303), pRSET-WHaloCaMP1a (205304), pRSET-WHaloCaMP1b-EGFP (205305), pRSET-WHaloCaMP-enOSpep-EGFP (205306), pAAV-synapsin-WHaloCaMP1a-EGFP (205307), pAAV-synapsin-WHaloCaMP1a (205308), pAAV-CaMKII-WHaloCaMP1a-EGFP (205309), pAAV-CaMKII-WHaloCaMP1a (205310), pTol2-elavl3-WHaloCaMP1a-EGFP (205311), pTol2-elavl3-WHaloCaMP1a (205312), pCAG-WHaloCaMP1a-EGFP (205313) and p10xUAS-WHaloCaMP1a-EGFP (205314).

Protein expression and purification

For expression and purification of proteins, T7 Express cells (New England Biolabs) were transformed with pRSET plasmids encoding the protein of interest. The bacteria were grown in auto-induction medium using the Studier method⁴⁵ with antibiotics at 30 °C for 48 h, shaking at 200 rpm. Cell pellets were collected by centrifugation and lysed in Tris-buffered saline (TBS) (19.98 mM Tris, 136 mM NaCl, pH 8.0) with *n*-octyl-β-D-thioglucopyranoside (5 g l⁻¹). Aggregates were disrupted by sonication, and the lysate was cleared by centrifugation. Protein purification was performed using an N-terminal poly-histidine (His₆) tag using HisPur Ni-NTA resin (Thermo Fisher Scientific) according to the manufacturer's recommendations. Purified proteins were buffer exchanged into TBS using Amicon concentration filters (Merck). Protein aliquots were stored at 4 °C or flash frozen and stored at -80 °C until assayed.

Polyacrylamide gel electrophoresis

To verify protein expression and covalent bond formation with HaloTag dye-ligand, proteins were run via sodium dodecyl sulfate-

polyacrylamide gel electrophoresis. Proteins were prelabeled with a 1.2-molar equivalence of dye-ligands before being separated on a NuPAGE 4–12%, Bis-Tris protein gel (Thermo Fisher Scientific). Imaging of in-gel fluorescence was performed using a ChemiDoc MP system (Bio-Rad) with epi-blue (460–490 nm), epi-green (520–545 nm) or epi-red (625–650 nm) excitation, and emission filters were set to 518–546 nm, 577–613 nm or 675–725 nm. PageBlue Protein Staining Solution (Thermo Fisher Scientific) was used to visualize the total protein amount in the gel.

Crystallography

For crystallization, HaloTag7 was further purified with a size-exclusion chromatography Superdex 200 10/300 GL column (GE Healthcare) at a flow rate of 0.5 ml min⁻¹ in 50 mM Tris-HCl, 75 mM NaCl, pH 7.4. The purified protein was incubated with 2 molar equivalents of the JF₆₆₉-HaloTag ligand for 5 h at 22 °C (room temperature), and excess dye-ligand was removed with PD MiniTrap desalting columns with Sephadex G-25 resin (Cytiva Life Sciences), pre-equilibrated with 50 mM Tris-HCl and 75 mM NaCl, pH 7.4. Crystallization was performed at 22 °C (room temperature), and crystals were grown using the sitting-drop vapor-diffusion method in 96-well plates using precipitant solutions from Crystal Screen Cryo HT (Hampton Research). HaloTag7₆₆₉ (10 mg ml⁻¹) was crystallized by mixing 1:1 (vol:vol) with a precipitant solution of 0.2 M ammonium phosphate monobasic, 0.1 M Tris, pH 8.5, 50% (vol/vol) (+/-)-2-methyl-2,4-pentanediol. Blue HaloTag7₆₆₉ crystals were plunged into liquid nitrogen for storage and transport. X-ray diffraction data were collected at beamline 8.2.2 at the Advanced Light Source, and a wavelength of 1 Å and a temperature of 100 K under a cold nitrogen stream were used. Diffraction data were integrated using xia2 (ref. 46) and DIALS⁴⁷ and scaled using Scala from the CCP4 suite⁴⁸. The structure was solved using Phaser⁴⁹, using a prior structure of HaloTag7 bound to the trimethyl rhodamine HaloTag7 ligand as a search module (PDB 6U32). Refinement was performed iteratively using REFMAC5 (ref. 50), and model rebuilding and adjustments were performed in Coot⁵¹. The refined structure of HaloTag7₆₆₉ (PDB 8SW8) exhibited good model geometry, with 94.9% of residues in the favored regions of the Ramachandran plot and 1% in disallowed regions.

Library construction

For directed evolution of WHaloCaMPs, the gene of interest fused to the sequence for EGFP as an expression marker was cloned in the desired geometry into the pRSET plasmid. NNS degenerate codons were used for single-site mutagenesis, and primers designed using the 22-codon trick⁵² were used for two-site mutagenesis. PCR was used to amplify the gene fragment including the degenerate codon site(s), and the NEBuilder HiFi kit (New England Biolabs) was then used according to the manufacturer's instructions. The reactions were diluted 1:3 before being electroporated into T7 Express *Escherichia coli*, which was plated on LB-ampicillin plates to isolate single colonies. Around 10–20 colonies were sequenced from each reaction to verify library generation.

Library bacterial lysate screen

For library expression, single colonies were picked and transferred to liquid growth medium in 96-well blocks containing 800 µl auto-induction medium and ampicillin (100 µg ml⁻¹). The blocks were shaken at 400 rpm for 48 h. The bacteria were then pelleted and lysed with three freeze-thaw cycles at -20 °C or -80 °C. The pellet was resuspended in 30 mM 3-morpholinopropane-1-sulfonic acid (MOPS), 100 mM KCl at pH 7.2, with shaking for 1 h at 37 °C, and the lysate was cleared by centrifugation. After clearing, 250 µl of the lysate was transferred into 96-well blocks of 10-µl pre-aliquoted solutions of 10 µM JF₆₆₉-HaloTag ligand in 30 mM MOPS, 100 mM KCl at pH 7.2 (final labeling concentration of the JF₆₆₉-HaloTag ligand was ~380 nM). Two 96-well black plates were prepared with a 'low' concentration of Ca²⁺ (5 µl, 10 mM CaCl₂ in 30 mM MOPS, 100 mM KCl

at pH 7.2) or a 'low' concentration of ethylene glycol-bis(β-aminoethyl ether)-*N,N,N',N'*-tetraacetic acid (EGTA) (5 µl, 20 mM EGTA in 30 mM MOPS, 100 mM KCl at pH 7.2). The JF₆₆₉-dye labeled lysate (95 µl) was transferred into the prepared 96-well plates (final concentration of low Ca²⁺ was 0.5 mM, and low EGTA was 1 mM), and fluorescence was read on a plate reader (Tecan Spark 20M) with a stacking module. Fluorescence was read at an excitation wavelength of 485 nm and an emission wavelength of 510 nm for EGFP and at an excitation wavelength of 670 nm and an emission wavelength of 690 nm for proteins labeled with JF₆₆₉ with a 5-nm bandgap. After an initial reading, the Ca²⁺ and EGTA conditions were interchanged: 20 µl of a solution with 100 mM EGTA was added to the 96-well plate containing Ca²⁺ at a low concentration, and 20 µl of a solution with 50 mM CaCl₂ was added to the 96-well plate containing EGTA at a low concentration. The fluorescence emission was again read on a plate reader (Tecan Spark 20M) with a stacking module. To identify top performing variants, variants above a threshold value of EGFP fluorescence were ranked by calculating ΔF/F₀ (where ΔF is the fluorescence intensity in Ca²⁺ fluorescence intensity in EGTA and F₀ is the fluorescence intensity in EGTA) of the JF₆₆₉ signal both in the 'low' Ca²⁺-EGTA and 'high' Ca²⁺-EGTA regimes. Depending on the library, 0–38 top hits were chosen, expanded from the pelleted lysate before labeling and sequenced by Sanger sequencing.

Library Ca²⁺ response validation

Unique sequences of top performing variants were expressed and purified using their N-terminal His₆-tag as described above. The concentration of the purified proteins was quantified using the absorbance of EGFP fused to the C terminal ($\epsilon_{488} = -55,000 \text{ cm}^{-1} \text{ M}^{-1}$). The variants were labeled with stoichiometric amounts of dye-ligand (15 µM purified protein with 10 µM JF₆₆₉-HaloTag ligand) for at least 1 h at 22 °C (room temperature). The labeled variants (2 µl) were aliquoted into 98 µl of 0.5 mM 'low' Ca²⁺ and 1 mM 'low' EGTA, and the fluorescence emission was read with a plate reader, recording both the EGFP and JF₆₆₉ fluorescence emission, as previously performed. The 'low' conditions were then changed to 'high' by adding 20 µl of 100 mM EGTA to the 'low' Ca²⁺ wells and 20 µl of 50 mM CaCl₂ to the 'low' EGTA wells, and fluorescence was read once again on the plate reader. The ΔF/F₀ value was calculated for each variant, both in the 'low' Ca²⁺-EGTA and 'high' Ca²⁺-EGTA regimes. The overall fluorescent intensity was compared to that of the HaloTag-EGFP label and read under the same conditions in the plate reader. The variants with the largest ΔF/F₀ value in the validation were further validated in a dye-ligand-capture assay by fluorescent polarization.

Fluorescence polarization dye-ligand-capture rate assay

To determine the dye-ligand-capture rate of the protein variants with the dye-HaloTag ligand, a fluorescence polarization assay was used. Purified protein was diluted into buffer containing 30 mM MOPS, 100 mM KCl, pH 7.2 and 0.5 mg ml⁻¹ BSA, with either 10 mM EGTA or 20 mM CaCl₂. Proteins were prepared at 625 nM, 312.5 nM, 156 nM and 78 nM. The diluted solutions (80 µl) were added to 96-well black-well plates. A solution of the JF₅₄₉-HaloTag ligand was prepared in 30 mM MOPS, 100 mM KCl, pH 7.2, 0.5 mg ml⁻¹ BSA, 10 mM EGTA at a final concentration of 62.5 nM. Fluorescence polarization was read over 5–20 min in a plate reader (Tecan Spark 20M) at 37 °C, after mixing 80 µl of the protein solutions with 20 µl of the dye-ligand solution with final protein concentrations of 500 nM, 250 nM, 125 nM and 62.5 nM and a final dye-ligand concentration of 12.5 nM. Excitation was set to 535 nm, and emission was set to 580 nm, with a bandwidth of 20 nm. The G factor was manually set to 1.79 after measuring a dilute concentration of dye-ligand in buffer with the same excitation and emission settings. The binding curve over time was fit with a single exponential in a custom-written Python script with `curve_fit` in `scipy.optimize`, where y is the fluorescence polarization in mP, Y_0 is the value

of y when intercepting the y axis, P_l is the value of y at plateau, k is the pseudo-first-order rate constant and x is the time in seconds.

$$y(x) = Y_0 + (P_l - Y_0) \times (1 - e^{-kx})$$

The pseudo-first-order rate constant was calculated for each protein concentration, and an apparent or calculated second-order rate constant for dye-ligand capture was calculated, where $k_{2,\text{calc}}$ is the calculated second-order rate constant in M⁻¹ s⁻¹, k is the pseudo-first-order rate constant and [protein] is the protein concentration during the run.

$$k_{2,\text{calc}} = \frac{k}{[\text{protein}]}$$

This plate reader assay was too slow to capture rates faster than 10⁶ M⁻¹ s⁻¹; however, we used it to verify that we had not lost the fast dye-ligand-capture rate for the variants.

General experimental information for synthesis

See Supplementary Note 2.

Ultraviolet-visible spectroscopy of protein-dye conjugates

To record absorbance spectra and molar extinction coefficients of WHaloCaMP bound to dyes, proteins were prelabeled with dye-HaloTag ligand. The dye-HaloTag ligand was reconstituted from lyophilized powder at 2 mM in dimethylsulfoxide (DMSO). For excess dye-ligand addition and subsequent removal, HaloTag or variants of WHaloCaMP were diluted to 50 µM in TBS, and dye-HaloTag ligand was added at a final concentration of 100 µM. After an incubation of at least 1 h at 22 °C (room temperature), excess dye-ligand was removed with a PD SpinTrap G-25 column (Cytiva Life Sciences), pre-equilibrated with 30 mM MOPS, 100 mM KCl at pH 7.2. After elution, the protein-dye concentration was quantified with a NanoDrop One^C UV-Vis spectrophotometer (Thermo) by reading the absorbance at 280 nm and using a calculated molar extinction coefficient at 280 nm (Expasy, ProtParam tool). Protein concentrations were around 40 µM. For stoichiometric labeling of the protein variants, 20 µM protein was diluted in TBS and labeled with 10 µM JF dye-HaloTag ligand. DMSO concentrations did not exceed 1% (vol/vol). The protein-dye conjugates were diluted to 1.5 µM in the two solutions from Calcium Calibration Buffer Kit #1 (Invitrogen) (0 and 10 mM CaEGTA, containing either 10 mM EGTA or 39 µM free Ca²⁺ in 30 mM MOPS, 100 mM KCl at pH 7.2). Absorption spectra were recorded on a Cary Model 100 spectrometer (Agilent) using 1-cm-pathlength semi-micro quartz cuvettes with self-masking sides (1-ml volume). Spectra were normalized to the maximum absorption in the presence of saturating Ca²⁺. For molar extinction measurements, protein-dye conjugates were further diluted in with the 0 mM or 10 mM CaEGTA buffer to 750 nM, 375 nM and 187 nM, and the absorbance spectra were recorded. The molar extinction coefficient at a particular wavelength was determined by performing a background correction and plotting the absorbance (y) against the concentration (x). The molar extinction coefficient (b) was taken to be the line fit through the points, with a y-intercept of a .

$$y(x) = a + bx$$

Fluorescence spectroscopy of protein-dye conjugates

To record fluorescence excitation and emission spectra, proteins were first prelabeled with dye-HaloTag ligand at a stoichiometric molar ratio. Protein (20 µM) was diluted in TBS and labeled with 10 µM JF dye-HaloTag ligand. DMSO concentrations did not exceed 1% (vol/vol). After incubation for at least 1 h at 22 °C (room temperature), the protein-dye conjugate was diluted in either 0 mM or 10 mM CaEGTA buffer. The final concentration of the protein-dye conjugate was 666 nM. Fluorescence spectra were recorded on a Cary Eclipse fluorometer (Agilent) using 1-cm-pathlength quartz spectrophotometer 3.5-ml

cuvettes. Spectra were normalized to the maximum fluorescence excitation or emission in the presence of saturating Ca^{2+} concentrations.

Two-photon spectroscopy of protein–dye conjugates

WHaloCaMP1a was prelabeled with a stoichiometric amount of dye (10 μM dye-ligand to 20 μM WHaloCaMP1a) for at least 1 h at room temperature. The protein–JF dye-ligand conjugates were then diluted to a final concentration of 1 μM of dye-ligand equivalence in either 0 mM or 10 mM CaEGTA buffers from Calcium Calibration Buffer Kit #1 (Invitrogen). Two-photon spectroscopy of WHaloCaMP–JF dye-ligand conjugates was performed as previously described^{11,53}. Briefly, an inverted microscope (IX81, Olympus) equipped with a $\times 60$ 1.2-numerical aperture (NA) water objective (Olympus) was used. To excite the samples, a pulsed 80-MHz Ti-sapphire laser (Chameleon Ultra II, Coherent) was used for 710–1,080 nm and an OPO (Chameleon Compact OPO, Coherent) was used for 1,000–1,500 nm. For excitation of WHaloCaMP1a₄₉₄ and WHaloCaMP1a₅₅₂, a dichroic filter (675DCSXR, Omega) and a shortpass filter (720SP, Semrock) were used, and emission was collected using a bandpass filter (539BP278, Semrock). By contrast, for WHaloCaMP1a₆₆₉ and WHaloCaMP1a₇₂₂, laser excitation was achieved through a dichroic filter (FF825-SDio1, Semrock) and emission was collected using a bandpass filter (709BP167, Semrock). Fluorescence detection was achieved with a fiber-coupled avalanche photodiode (SPCM-AQRH-14, PerkinElmer). All the fluorescence excitation spectra are corrected for the wavelength-dependent transmission of the dichroic and bandpass filters and quantum efficiency of the detector. The corrected spectra were used to calculate the action cross-section using fluorescein⁵⁴, rhodamine B⁵⁵ and styryl 9M⁵⁵ as a reference. Spectra are averages ($n = 2$).

Quantum yield determination of protein–dye conjugates

To record quantum yields, proteins were first prelabeled with JF dye-HaloTag ligand at a stoichiometric molar ratio. The protein–dye-ligand conjugates were diluted in either 0 mM or 10 mM CaEGTA buffer. A Quantaurus-QY spectrometer (model C11374, Hamamatsu) with an integrating sphere was used, measurements were performed on dilute samples ($A < 0.1$), and self-absorption corrections were performed⁵⁶ using the instrument software.

Ca^{2+} titrations

To determine the Ca^{2+} affinity and cooperativity of the WHaloCaMP sensors, Ca^{2+} titrations were performed with a commercial Calcium Calibration Buffer Kit #1 (Invitrogen) with 0 mM and 10 mM CaEGTA. Proteins were prelabeled with excess dye-HaloTag ligand, and any excess dye-ligand was removed with a PD SpinTrap G-25 column (Cytiva Life Sciences), pre-equilibrated with 30 mM MOPS, 100 mM KCl at pH 7.2. The prelabeled protein–dye conjugate (2 μl) was diluted into 98 μl of a premixed solution of CaEGTA in black 96-well plates. Fluorescence intensities were read in a plate reader (Tecan Spark 20M). For WHaloCaMP1a₄₉₄, excitation was 490 nm and emission was 530 nm. For WHaloCaMP1a₅₅₂, excitation was 560 nm and emission was 580 nm. For WHaloCaMP1a₆₆₉, excitation was 670 nm and emission was 690 nm. For WHaloCaMP1a₇₂₂, excitation was 730 nm and emission was 750 nm. All bandwidths were set to 5 nm. The free Ca^{2+} concentration was calculated, taking the dissociation constant of EGTA for Ca^{2+} to be 150 nM at 22 °C and pH 7.2 (ref. 57). Changes in fluorescence on addition of Ca^{2+} were calculated in Microsoft Excel. The fluorescence (y) was plotted against the free Ca^{2+} concentration (x), and a four-parameter dose-response curve (variable slope) using GraphPad Prism software was fit in which a is the value of fluorescence at the bottom of the curve, b is the value of fluorescence at the top of the curve, EC_{50} is the concentration of agonist that gives a response halfway between the bottom and the top, and h is the Hill or cooperative coefficient.

$$y(x) = a + \frac{x^h \times (b - a)}{x^h + \text{EC}_{50}^h}$$

pH sensitivity of probes in vitro

Proteins were prelabeled with dye-HaloTag ligand at a stoichiometric molar ratio: 20 μM protein was diluted in TBS and labeled with 10 μM dye-HaloTag ligand. Labeled protein was then diluted into the following buffer systems containing 1 mM CaCl₂ or 50 mM EGTA: citrate (pH 4.0–6.2), phosphate (pH 5.8–8.0) and Tris (pH 7.8–9.0), all with 10 mM buffer and 150 mM NaCl. Protein (2 μl) was diluted into the buffer in 96-well black plates, and fluorescence was read with a plate reader (Tecan Spark 20M).

Stopped-flow kinetic measurements of Ca^{2+} kinetics

Ca^{2+} unbinding kinetics of WHaloCaMPs were determined using a Photophysics SX20 stopped-flow device. The prelabeled protein (~1.3 μM) was rapidly mixed with a solution of 30 mM MOPS, 100 mM KCl, 10 mM EGTA, pH 7.2 in a 1:1 ratio. The sensors were excited using a light-emitting diode (LED; 625 nm), and fluorescence emission was collected through a 665-nm longpass filter. Fluorescence decay was fit with the decay curves described in Supplementary Fig. 2.

One-photon widefield bleaching of WHaloCaMP1a₆₆₉

One-photon bleaching experiments were performed with an inverted Nikon Eclipse Ti2 microscope as previously described⁵⁸. Briefly, bleaching experiments were carried out in aqueous droplets of purified protein labeled with dye-ligand isolated in 1-octanol⁵⁹. Labeled purified protein was diluted to 500 nM using the commercial Calcium Calibration Buffer Kit #1 (Invitrogen) with 0 mM and 10 mM CaEGTA and supplemented with 0.3 mg ml⁻¹ BSA. This solution was diluted tenfold in a 1-octanol–PBS suspension and agitated by tapping. The solution was placed on a pre-silanized glass slide and sandwiched with a coverslip. The microdroplets were illuminated using a $\times 40$ (NA = 1.3, Plan Fluor, Nikon (field number (FN) = 25.2)) oil-immersion objective. Illumination was provided by an LED (Spectra X Light Engine, Lumencor) and imaged through the following filter cube (89000, Chroma), ET645/30x, 89100bs, ET705/72m. Images were captured with a scientific complementary metal-oxide semiconductor (sCMOS) camera (ORCA-Flash4.0, Hamamatsu), and images were acquired with 1 s of exposure every 2 s. Power at the objective was measured with a microscope slide power sensor (S170C, Thorlabs) to 7 mW, giving an irradiance of 23 mW mm⁻². Each sample was bleached continuously for 6.6 min. Background subtraction was performed in Fiji⁶⁰; fluorescence emission was normalized to the first frame. One-phase decay was fit to the data in GraphPad Prism software.

Primary neuronal culture and labeling with dye-HaloTag ligand

Procedures involving rodent animals were conducted in accordance with protocols approved by the Howard Hughes Medical Institute Janelia Research Campus Institutional Animal Care and Use Committee and Institutional Biosafety Committee. Hippocampal neurons were extracted from P0–P1 Sprague-Dawley rat pups and plated into 24-well glass-bottom plates or 35-mm dishes (MatTek, #1.5 coverslip). A coating of poly-D-lysine was applied before plating the cells. Neurons were cultured at 37 °C with 5% CO₂ in a humidified atmosphere in NbActiv4 medium (BrainBits). After plating (3–4 d), neurons were transduced with AAV1 virus to express the gene of interest under the human SYN1 (*hsyn1*) promoter. After transduction (17–21 d), the neurons were labeled with dye-HaloTag ligand. Dye-HaloTag ligands were first dissolved to make 2 mM stock solutions in DMSO from lyophilized powder. The neurons were labeled with 50–100 nM dye-HaloTag ligand at 37 °C for 30–45 min. The neurons were then washed with imaging buffer containing 145 mM NaCl, 2.5 mM KCl, 10 mM glucose, 10 mM HEPES (pH 7.4), 2 mM CaCl₂ and 1 mM MgCl₂. After three washes, imaging buffer containing synaptic blockers⁶¹ (10 μM 6-cyano-7-nitroquinoxaline-2,3-dione, 10 μM 3-(2-carboxypiperazin-4-yl)propyl-1-phosphonic acid, 10 μM gabazine and 1 mM (S)- α -methyl-4-carboxyphenylglycine) was

added to block ionotropic glutamate, γ -aminobutyric acid and metabotropic glutamate receptors.

Field stimulation of WHaloCaMP1a in primary neuronal culture

Field stimulation of neurons was performed using a platinum wire electrode inserted in the medium, controlled by a high-current isolator (A385, World Precision Instruments) set at 90 mA. Trains of APs were delivered to the platinum wire electrode from one to 160 APs, at intervals described in each imaging modality. Unless otherwise stated, the fluorescent traces from hand-segmented neurons from at least three fields of view from at least two separate neuron batches were extracted in Fiji⁶⁰. $\Delta F/F_0$ values were calculated, with F_0 being the average fluorescence recorded 1 s before each stimulus. Cells with $\Delta F/F_0 > 0$ were used. The signal-to-noise ratio was calculated from the amplitude in the fluorescent change on the field stimulation divided by the standard deviation of the baseline fluorescence 1 s before each stimulus. Calculated time to peak was calculated from the onset of stimulus to the maximal fluorescence value. The $t_{1/2}$ of decay was calculated by fitting a two-phase decay in GraphPad Prism software to the $\Delta F/F_0$ trace after the field stimulus had stopped.

Widefield imaging in the visible spectrum

Widefield imaging in the visible spectrum (up to 700 nm) was performed on an inverted Nikon Eclipse Ti2 microscope with a $\times 20$ air objective (NA = 0.75, Nikon) equipped with a Spectra X Light Engine (Lumencore) and imaged with an ORCA-Flash4.0 sCMOS camera (Hamamatsu). The Spectra X Light Engine was equipped with 485/25-nm, 550/15-nm and 640/30-nm excitation filters for exciting WHaloCaMP₄₉₄, WHaloCaMP₅₅₂ and WHaloCaMP₆₆₉. A quad bandpass (set number 89000, Chroma) with 490/20-nm, 555/25-nm and 645/30-nm excitation filters, a dichroic mirror (89100bs, Chroma) and 525/36-nm, 605/52-nm and 705/72-nm emission filters (Chroma) were also used. Imaging was performed at 33 Hz, and the field stimulation was controlled with an Arduino Uno board synchronized with light sources in Nikon Elements software. A train of 1, 2, 3, 5, 10, 20, 40, 80, 120 and 160 APs with a pulse duration of 1 ms at 80 Hz were elicited with 20-s time intervals between each stimulation.

Widefield imaging in the near-infrared

For imaging WHaloCaMP1a₇₂₂ in the near-infrared, we used a custom-built upright microscope as previously described⁶² with modifications. Neurons expressing WHaloCaMP1a and labeled with the JF₇₂₂-HaloTag ligand were imaged using a $\times 40$ objective (Nikon N40X-NIR, 0.8 NA and a working distance of 3.5 mm). To excite WHaloCaMP1a₇₂₂, we used a 671-nm laser (gem 671, Laser Quantum). To image the EGFP expression marker, we used a four-wavelength LED light source (Thorlabs, LED4D067), using the LED at 470 nm. We used an imaging dichroic beam splitter with edge at 699 nm (FF699-FD101-T1-25x36, Semrock) and a 715-nm emission filter (FF01-715/LP-25, Semrock) to clean up the fluorescence signal before detection by camera. Both visible and near-infrared fluorescence signals were imaged using an InGaAs camera with optimized sensitivity in the NIR-SWIR range (Ninox 640 II, Raptor Photonics). Images were acquired using μ Manager, an open-source microscopy software⁶³. Images were acquired at 10 frames per second with 400–500 frames for each run. We performed field stimulation with the stimulation controlled using the MATLAB-based waveform generator WaveSurfer to elicit 1, 5, 10, 20 or 160 APs with a pulse duration of 1 ms and a square pulse train at 80 Hz and analyzed the data as described under ‘Field stimulation of WHaloCaMP1a in primary neuronal culture’.

Simultaneous electrophysiology and fluorescence imaging in primary neuron culture

All imaging and electrophysiology measurements were performed in imaging buffer. Internal solution for current-clamp recordings

contained the following: 130 mM potassium methanesulfonate, 10 mM HEPES, 5 mM NaCl, 1 mM MgCl₂, 1 mM magnesium ATP, 0.4 mM sodium GTP and 14 mM Tris-phosphocreatine, adjusted to pH 7.3 with KOH and adjusted to 300 mOsm with sucrose. Glass capillaries with filaments (Sutter Instrument) were pulled to a tip resistance of 4–6 M Ω .

Pipettes were positioned with an MPC-200 manipulator (Sutter Instrument). An EPC 800 amplifier (HEKA) was used for acquiring electrophysiology recordings, filtered at 10 kHz with an internal Bessel filter and digitized using a National Instruments PCIe-6353 acquisition board at 20 kHz. Data were acquired from cells with access resistance <25 M Ω . WaveSurfer software was used to generate the various analog and digital waveforms to control the amplifier, the camera and light source and record voltage and current traces. Cells were initially held at -70 mV. A 440-nm light pulse (5 ms, 10 Hz at 0.45 mW mm⁻² when CheRiff was coexpressed with WHaloCaMP1a) or current injection (when only WHaloCaMP1a was expressed) was applied to evoke APs and initiate Ca²⁺ entry into the cell.

Light (640 nm at 0.76 mW mm⁻²) was used to excite WHaloCaMP1a with an emission filter at 705/72 nm. Light (555 nm at 1.39 mW mm⁻²) was used for excitation of jRCaMP1a, and emitted fluorescence was filtered with a 607/70-nm emission filter. Fluorescence images were collected using an sCMOS camera (ORCA-Flash4.0, Hamamatsu), and image acquisition was performed using HClImage Live (Hamamatsu) with frame rate at 30 Hz.

Current-clamp recording of CheRiff with different wavelengths of light

For testing CheRiff’s response to longer wavelength stimulation, 555-nm and 640-nm light was applied for 1 s to illuminate CheRiff-expressing neurons, and voltage signals were monitored. Light powers were measured using a power meter (Thorlabs, PM100A) with an Si photodiode (Thorlabs, S120C or S170C).

Two-photon imaging of acute mouse slices with WHaloCaMP1a

All procedures for rodent husbandry and surgery were performed following protocols approved by the Washington University Institutional Animal Care and Use Committee and in accordance with National Institutes of Health guidelines. The sequence for FLIM-AKAR, together with a transcriptional stop codon flanked by *loxP* sites, was knocked in at the ROSA26 locus (JAX 039003)²⁶. These mice were subsequently crossed with *Emx1*^{IRES-Cre} mice (JAX 005628)⁶⁴ to create mice homozygous for both *Emx1*-Cre and the sequence for FLIM-AKAR at their respective loci. We did not select for males or females specifically for the experiment. Mice were kept on a 12-h light–dark cycle, with humidity between 30% and 70% and a temperature of 20–26 °C.

WHaloCaMP1a was delivered via stereotaxic injections. AAV1-CAMKII-NES-WHaloCaMP1a (5×10^{12} virus molecules per ml) was delivered using a UMP3 microsyringe pump (World Precision Instruments) via glass pipette to P0 or P1 pups. A total of 200 nl per pup was delivered at ten different coordinates (20 nl per coordinate) at a rate of 20 nl s⁻¹. The coordinates are as follows, relative to lambda in millimeters: (1) anterior, 1.2; lateral, 1.2; depth from the skin, 1.2, 0.8, 0.4, (2) anterior, 0.8; lateral, 1.5; depth from the skin, 1.5, 1.0, 0.5, and (3) anterior, 0.5; lateral, 2.0; depth from the skin, 2.0, 1.5, 1.0, 0.5.

The JF₆₆₉-HaloTag ligand fluorescent dye was delivered either by r.o. injection into mice before acute slicing or by incubation of acute brain slices (from dye-naive mice) in dye-infused artificial cerebrospinal fluid (ACSF; see composition below). For r.o. injection, a total of 200 nmol JF₆₆₉-HaloTag ligand was first dissolved in 20 μ l DMSO and subsequently diluted with 20 μ l of 20% Pluronic in DMSO (Fisher) and 90 μ l PBS (Corning). Imaging was performed within 24 h of dye injection. For acute slice incubation, 100 nmol JF₆₆₉-HaloTag ligand was reconstituted in 20 μ l DMSO and mixed with ACSF to create a 0.0626–0.25 μ M solution. Acute brain slices were incubated in this

dye–ACSF solution for 30 min and were subsequently washed with dye-free ACSF for at least 30 min before imaging.

Mice were anesthetized with isoflurane and subsequently euthanized. All solutions were bubbled with carbogen (5% CO₂ and 95% O₂) before use, and ACSF was continuously bubbled while in use. Mice aged P25 or younger were sectioned in cold sucrose cutting solution (containing (in mM): 87 NaCl, 25 NaHCO₃, 1.25 NaH₂PO₄, 2.5 KCl, 75 sucrose, 25 glucose, 1MgCl₂). Mice aged P30 or older underwent intracardiac perfusion with cold ACSF (containing (in mM): 127 NaCl, 2.5 KCl, 25 NaHCO₃, 1.25 NaH₂PO₄, 2 CaCl₂, 1MgCl₂ and 25 glucose). Their brains were rapidly dissected and sectioned in cold choline cutting solution (containing (in mM): 25 NaHCO₃, 1.25 NaH₂PO₄, 2.5KCl, 7MgCl₂, 25 glucose, 0.5 CaCl₂, 110 choline chloride, 11.6 ascorbic acid, 3.1 pyruvic acid). Acute coronal slices were collected at a thickness of 300 μm with a Leica VT1000 S vibratome.

After sectioning, slices from both groups were transferred to ACSF for recovery at 34 °C for 5–10 min. After recovery, the slices were kept in ACSF at room temperature. Once ready for imaging, the slices were transferred to a microscope chamber where they were perfused with ACSF at a flow rate of 2–4 ml min⁻¹.

A custom-built microscope was used to perform two-photon imaging in acute brain slices. WHaloCaMP1a₆₆₉ was excited at a wavelength of 1,250 nm, and FLIM-AKAR was excited at 920 nm. Two mode-locked laser sources were used in an alternating fashion to excite WHaloCaMP1a₆₆₉ (Spectra-Physics, InSight X3, 80 MHz) and FLIM-AKAR (Spectra-Physics, Mai Tai HP Ti:Sapphire, 80 MHz), respectively. Photons were collected with fast photomultiplier tubes (PMTs; Hamamatsu, H10770PB-40) with a ×60 objective (Olympus, NA1.1). Image acquisition was accomplished with ScanImage⁶⁵, a custom-written software, in MATLAB 2012b.

FLIM was performed as described previously with FLIM-AKAR^{24–26}. The FLIM board used was SPC-150 (Becker & Hickl), and time domain single-photon counting was performed in 256 time channels. Intensity Ca²⁺ imaging was performed with WHaloCaMP1a₆₆₉. Neurons with nuclear-excluded basal WHaloCaMP1a₆₆₉ signals were used for experiments. Pixel images (128 × 128) were collected.

Both sensors' emission light was collected through a 580-nm dichroic mirror (FF580-FDi01-25x36, Semrock), followed by a 525/50-nm bandpass filter (FF03-525/50-25, Semrock) for FLIM-AKAR or a 690/50-nm bandpass filter (ET690/50m, Chroma) for WHaloCaMP1a₆₆₉.

All acute slice experiments were performed in the presence of 1 μM DPCPX to inhibit adenosine receptors and 1 μM tetrodotoxin to block APs.

All chemicals were added to acute slices by addition into the perfusion reservoir. The final concentrations of chemicals are as follows: (+)-muscarine iodide (Mus), 10 μM, from Tocris; tetrodotoxin citrate, 1 μM, from Hello Bio; DPCPX, 1 μM, from Tocris; forskolin (FSK), 50 μM, from Cayman Chemical; potassium chloride, 55 mM, from Cayman Chemical.

The ROI for each neuronal cell body was manually selected. An ROI for background fluorescence with no cellular processes was similarly selected. The fluorescence signal for all pixels in a neuron's ROI was averaged, and the average background fluorescence was subtracted from it. The resulting net fluorescence was plotted against time. The ΔF/F₀ was calculated as (F – F₀)/F₀, where F₀ is the fluorescence signal averaged over the entire baseline period.

The amplitudes of intensity changes were quantified as follows:

Baseline_{start} = average ΔF/F₀ of first three intensity acquisitions of baseline

Baseline_{end} = average ΔF/F₀ of last three intensity acquisitions of baseline

Mus_{end} = average ΔF/F₀ of last three intensity acquisitions of muscarine-only application;

Baseline_{max} = maximum ΔF/F₀ recorded during baseline;

Mus_{max} = maximum ΔF/F₀ recorded during muscarine-only application;

FSK_{max} = maximum ΔF/F₀ recorded during forskolin application;

Max ΔBaseline = MaxBaseline – Baseline_{start};

Max ΔMus = Mus_{max} – Baseline_{end};

Max ΔFSK = FSK_{max} – Mus_{end}.

For presentation purposes, the WHaloCaMP1a₆₆₉ line was smoothed and presented alongside the raw data. Smoothing was performed in GraphPad Prism, using six neighboring points and a second-order polynomial for smoothing.

FLIM curve fitting, calculation of average lifetime over an ROI and ROI analysis were performed as described previously²⁵. The amplitudes of cytoplasmic lifetime changes were quantified as follows:

Baseline_{start} = average lifetime of the first three acquisitions of baseline;

Baseline_{end} = average lifetime of the last three acquisitions of baseline;

Baseline_{min} = minimum lifetime during baseline;

Mus_{end} = average lifetime of the last three acquisitions of muscarine only application;

Mus_{min} = minimum lifetime during muscarine only application;

FSK_{min} = minimum lifetime during forskolin application;

Max ΔBaseline = Baseline_{min} – Baseline_{start};

Max ΔMus = Mus_{min} – Baseline_{end};

Max ΔFSK = FSK_{min} – Mus_{end}.

WHaloCaMP imaging in living adult flies using widefield epifluorescence microscopy

Experiments were performed on 2–10-d-old heterozygous progeny of a cross between a mushroom body driver (R13F02-Gal4) and the two WHaloCaMP variants 10XUAS-NES::WHaloCaMP1a::EGFP-P10 in VK00005 and 10XUAS-NES::WHaloCaMP1b::EGFP-P10 in VK00005. jRGECO1a (20XUAS-IVS-NES-jRGECO1a-p10 in VK00005), which shares excitation and emission spectra with JF₅₅₂, was used as a comparison.

Dissections of head-fixed flies and dye-ligand incubation were performed similarly as in Volttron experiments⁵⁸. Briefly, a small window was opened in the head cuticle, and fat tissue and trachea that overlaid the mushroom body calyx region were removed. The exposed brain was bathed in a drop (~200 μl) of dye-containing saline (5 μM for JF₆₆₉-HaloTag ligand and 1 μM for JF₅₅₂-HaloTag ligand) for 1 h. Saline contained (in mM) NaCl, 103; KCl, 3; CaCl₂, 1.5; MgCl₂, 4; NaHCO₃, 26; N-Tris(hydroxymethyl)methyl-2-aminoethanesulfonic acid, 5; NaH₂PO₄, 1; trehalose, 10; and glucose, 10 (pH 7.3 when bubbled with 95% O₂ and 5% CO₂), 275 mOsm. The brain was then washed with fresh saline several times and maintained in the saline for 1 h. Imaging was performed on a widefield fluorescence microscope (SOM, Sutter Instrument) equipped with a ×60, 1.0-NA, water-immersion objective (LUMPlanFl/IR, Olympus) and an sCMOS camera (ORCA-Flash4.0 version 3, Hamamatsu). Images

of 256×256 pixels were acquired at 10 Hz with 4×4 binning with Hamamatsu imaging software (HClImage Live). Illumination was provided from an optical beam-combining system (LB-OBC-LLG, Sutter) equipped with a 660-nm LED (FG-OBC-660, Sutter) with an excitation filter (FF01-660/13-25-STR, Semrock) and a 561-nm LED (FG-OBC-561, Sutter) with an excitation filter (FF01-554/23-25-STR, Semrock). As the incidence angles were arranged at 18° in the four-beam combiner, the bandpass spectra of the excitation filters were shifted toward a shorter wavelength by 5–10 nm (SearchLight Spectra Viewer modeling). For WHaloCaMP₆₆₉, the 660-nm LED was used, and intensity at the sample plane was $\sim 0.64 \text{ mW mm}^{-2}$; emission was separated from excitation light using a dichroic mirror (FF677-Di01-25/36, Semrock) and an emission filter (FF01-719/60-25, Semrock). For WHaloCaMP₅₅₂ and jRGECO1a, the 561-nm LED was used, and intensities at the sample plane were $\sim 0.50 \text{ mW mm}^{-2}$ and $\sim 0.17 \text{ mW mm}^{-2}$, respectively; emission was separated from excitation light using a dichroic mirror (FF562-Di03-25x36, Semrock) and an emission filter (FF01-590/36-25, Semrock).

Odors used were 3-octanol (218405-50G, Sigma-Aldrich), 4-methylcyclohexanol (153095-250ML, Sigma-Aldrich) and apple cider vinegar (Heinz). Odors were diluted using a two-step, air dilution-based olfactometer²⁷ to a final concentration of 1:16 and delivered to flies at 200 ml min^{-1} for 2 s.

Data were analyzed in MATLAB with a custom script. Images were registered to correct for *x*-*y* movement. ROI corresponding to the calyx were manually selected, and the mean intensity of the ROI was extracted. F_0 was calculated as the mean over the 5 s of the imaging session before odor onset. Mean odor responses were integrated over a time window from 0.5 s and 5.5 s after odor onset.

Mice

All experimental protocols at Janelia Research Campus were conducted according to the National Institutes of Health guidelines for animal research and were approved by the Institutional Animal Care and Use Committee at Janelia Research Campus, Howard Hughes Medical Institute. All experimental protocols at the University of Maryland, Baltimore, were conducted according to the National Institutes of Health guidelines for animal research and approved by the Institutional Animal Care and Use Committee at the University of Maryland, Baltimore.

For two-photon experiments with WHaloCaMP1a₆₆₉, male mice (C57BL/6J background) aged 2–4 months were used (stock 000664, Jackson Laboratory). Mice were group housed with littermates until craniotomy surgery, after which they were singly housed. Mice were maintained on a 12–12-h (6 a.m.–6 p.m.) light–dark cycle. The holding room temperature was $21 \pm 1^\circ\text{C}$ with a relative humidity of 30% to 70%. Irradiated rodent laboratory chow (LabDiet 5053) was provided ad libitum.

For two-photon experiments with WHaloCaMP1a₅₅₂, male mice (C57BL/6J background) aged 2–4 months were used in this study (stock 000664, Jackson Laboratory). Mice were group housed with littermates in temperature- and humidity-controlled rooms with ad libitum access to water and rodent chow (PicoLab Rodent Diet 20, 5053 tablet, LabDiet–Land O'Lakes) on a 12-h light–dark cycle (9 p.m.–9 a.m., dark cycle and 9 a.m.–9 p.m., light cycle).

Retro-orbital injection of JF dye-ligands to mice

Retro-orbital injection of dye-HaloTag ligands was performed as previously described¹⁰ with minor modifications. The lyophilized dye-HaloTag ligand (200 nmol) was suspended in 20 μl DMSO. After vortexing, 20 μl of 20% Pluronic in DMSO was added, and the solution was pipetted up and down carefully to not form bubbles. PBS (80 μl ; 137 mM NaCl, 10 mM phosphate, 2.7 mM KCl, pH 7.4) was carefully added to the solution and before letting the solution sit for 10 min to let foam and bubbles settle. This solution (100 μl) was injected into one eye of an anesthetized mouse using a 0.5-ml 27G syringe to the r.o. sinus.

Two-photon imaging of WHaloCaMP1a₆₆₉ in the mouse visual cortex

Adult C57/BL6 male mice (2–4 months old) were used. Four mice were prepared and imaged. Representative images from two mice are presented in the article. Viral injections (300 nl, 400 μm below the brain surface) were performed, followed by implantation of a 4-mm cranial window as described previously⁶⁶, and r.o. injection of dye-ligands was performed 24 h before imaging.

Two-photon imaging of WHaloCaMP1a₆₆₉ in the mouse visual cortex using long-wavelength light was performed on a customized adaptive optics two-photon microscope based on the Thorlabs Bergamo II microscope, previously described¹⁹. Mice were anesthetized with isoflurane using a precision vaporizer, 3% (vol/vol) in oxygen for induction and 0.5–2% (vol/vol) during visual stimulation. The mouse was placed in a custom-built goniometric heated holder to restrict movement and maintained a body temperature of 37°C . Excitation was provided from a Coherent Discovery NX TPC. The objective was an Olympus XLUMPFLN objective, $\times 20$, 1.0 NA with water immersion. Excitation was performed at 950 nm (25% of light at laser source) for EGFP and at 1,225 nm (100% of light at laser source) for WHaloCaMP1a₆₆₉. Power ranged from 2 to 30 mW for 950 nm and from 5 to 15 mW for 1,225 nm. Emitted light was separated from excitation light via a 735-nm longpass dichroic and then filtered through a 525/50-nm bandpass dichroic (green PMT) and a 690/60-nm bandpass dichroic (near-infrared PMT). Light was collected via two Thorlabs PMT2100 PMTs and digitized via a laser-paced National Instruments DAQ card controlled by ScanImage⁶⁵ 2020 (Vidrio Technologies). Imaging parameters were 512×512 pixels with 44.8 frames per second at 2 \times zoom for a 200×200 - μm field of view. Visual stimulation was displayed on an LCD screen placed 10 cm in front of the mouse's eye, and moving bar stimuli were generated in MATLAB using Psychtoolbox²⁰ (with 8 s on, 8 s off) in eight equally spaced directions spaced by equal time periods of mean luminance and were shown to the animal synchronized with the acquisition. Light from the visual stimulation screen was filtered so that it minimally impacted the red and green PMT channels. Functional images were analyzed in Suite2p²¹, and fluorescent traces were calculated with F_0 as the lowest 0.5 percentile, calculating a rolling mean over 22 frames (0.5 s).

Two-photon imaging of WHaloCaMP1a₅₅₂ in the mouse visual cortex

Adult C57/BL6 male mice (2–4 months old) were used. The experiments were performed on four mice. A craniotomy 3.5 mm in diameter was first made over the left V1 of mice. Next, 40 nl of virus-containing solution (AAV2/1.CAMK2.NES-WHaloCaMP1a-EGFP, 9×10^{12} infectious units per ml) was injected 0.5 mm below the pia into the left V1 at four injection sites at the intersection points of the two left–right lines at bregma -3.4 mm and -4.0 mm and two anterior–posterior lines at 2.2 mm and 2.6 mm from the midline over 2 min. After the pipette was pulled out of the brain, a glass window made of a single coverslip (Fisher Scientific, no. 1.5) was embedded in the craniotomy and sealed in place with dental acrylic. A titanium headpost was then attached to the skull with cyanoacrylate glue and dental acrylic.

Visual stimuli were presented with a tablet monitor (Sceptre) displaying only blue light. The screen was positioned 15 cm from the right eye, covering $70^\circ \times 70^\circ$ of visual space and oriented at $\sim 40^\circ$ to the long body axis of the animal. Visual stimuli were generated using custom-written codes based on Psychophysics Toolbox⁶⁷ in MATLAB (Mathworks). During visual stimulation, the luminance level was kept constant. Each stimulus trial consisted of an 8-s blank period (uniform gray display at mean luminance), followed by 8 s of drifting grating (0.05 cycles per degree, temporal frequency of 1 Hz, eight randomized different directions). Each oriented drifting grating was presented for a total of five trials. Imaging was synchronized with ScanImage to start 4 s after the onset of the gray session for 8 s. Therefore, each imaging session covers 4 s of gray screen and 4 s of the drifting grating period.

Mice were kept on a warm blanket (37 °C) and anesthetized using 0.5% isoflurane and sedated with chlorprothixene (20–30 µl at 0.33 mg ml⁻¹, intramuscular). Imaging was performed with a custom-built two-photon microscope with a resonant scanner. Imaging was performed 4 weeks after virus injection and 24 h after r.o. injection of the dye-ligand. Each experimental session lasted 45 min to 2 h. Multiple sections (imaging planes) may be imaged within the same mouse. Fluorophores were excited by a different wavelength with a femtosecond laser system (Chameleon Discovery, Coherent) that was focused by an Olympus ×25, 1.05-NA objective. Emitted fluorescence photons reflected off a dichroic longpass beam splitter (FF705-Di01-25x36, Semrock) and were split with a dichroic mirror (S65DCXR, Chroma) and detected by PMTs H16201P-40//004, Hamamatsu) after filtering with a 510/84-nm filter (84-097, Edmund) for the green channel and two 750SP filters (64-332, Edmund) for the red channel. Images were acquired using ScanImage⁶⁵ (Vidrio Technologies). Functional images (512 × 512 pixels, 268 × 268 µm²) of L2/L3 cells (50–300 µm under the pia mater) were collected at 15 Hz. For 850 nm, post-objective laser power was 15 mW for imaging 148–210 µm deep in the brain. For 1,050 nm, post-objective laser power between 92 and 140 mW was used depending on the depth (100–362 µm) of cells.

Imaging data were processed with custom programs written in MATLAB (Mathworks) and Fiji⁶⁰. Images were registered with an iterative cross-correlation-based registration algorithm⁶⁸. All identifiable cell bodies were outlined by hand as ROI. The averaged fluorescence signal within the ROI was calculated as the raw ROI signal, F_{raw} . Neuropil subtraction was performed as follows. First, a square neuropil region, centered on an ROI, was determined by adding seven pixels to the width and height of the ROI, while excluding a two-pixel gap between the ROI and the neuropil region. Next, the average fluorescence signal of the neuropil excluding the ROI was calculated as the raw neuropil signal F_{neuropil} . The neuropil signal was then baseline subtracted by subtracting the average of the lowest 5% values of the neuropil signal time trace to obtain $\Delta F_{\text{neuropil}}$. Neuropil subtracted fluorescence signal within the ROI was then calculated⁶⁹ as $F = F_{\text{raw}} - 0.7 \times \Delta F_{\text{neuropil}}$. We calculated $\Delta F/F_0 = (F - F_0)/F_0$, where F is the instantaneous fluorescence signal and F_0 is the average fluorescence in the interval 4 s before the start of the visual stimulus. Visual responses were measured for each trial as $\Delta F/F_0$, averaged over the stimulus period. Visually responsive neurons were defined as cells with significant stimulus-related fluorescence changes (ANOVA across blank and eight direction periods, $P < 0.01$) with an average $\Delta F/F_0$ at preferred orientations greater than 10%. The fraction of cells detected as responsive was calculated as the number of significantly responsive cells over all the ROI analyzed. The cumulative distribution of peak $\Delta F/F_0$ responses included the maximal response amplitude from all analyzed cells, calculated as described above for each cell's preferred stimulus. The orientation selectivity index (OSI) was calculated as described before^{69,70} by fitting the fluorescence response from individual cells to the eight drifting grating stimuli with two Gaussians, centered at the preferred response angle (R_{pref}) and the opposite angle (R_{opp}). The OSI was calculated as:

$$\text{OSI} = \frac{R_{\text{pref}} - R_{\text{orth}}}{R_{\text{pref}} + R_{\text{orth}}},$$

where R_{orth} is the angle orthogonal to the preferred angle.

Standard functions and custom-written scripts in MATLAB were used to perform all analyses. The data were tested for normal distribution. Parametric tests were used for normally distributed data, and nonparametric tests were applied to all other data. Bar graphs and mean ± s.e.m. were used to describe data with normal distribution, while box plots and median ± interquartile range (IQR) were used to describe non-normally distributed data. Box plots represent the median and 25th–75th percentiles, and their whiskers are shown in Tukey style (±1.5 × IQR). A nonparametric test (Wilcoxon signed-rank

test) was used to examine paired data. Direct nonpaired comparisons between two groups were made using the Wilcoxon rank-sum test for non-normally distributed data. Statistical significance was defined as * $P < 0.05$, ** $P < 0.01$, *** $P < 0.001$. Experiments were not performed blind. Sample sizes were not predetermined by statistical methods but were based on those commonly used in the field. Medians, IQR, means and s.e.m. are reported throughout the text.

One-photon widefield imaging of WHaloCaMP1a₆₆₉–EGFP versus iGECI–EGFP

Adult C57/BL6 male mice (2–4 months old) were used. Four mice were prepared, and three mice were imaged. Representative images from two mice are presented in the article. A craniotomy 3 mm in diameter was first made over the right-whisker somatosensory cortex (barrel cortex) of mice. Virus-containing solution (300 nl; AAV1.CAMK2.NES-WHaloCaMP1a-EGFP or AAV1.CAMK2.NES-iGECI-EGFP (10¹² infectious units per ml)) was injected 0.3 mm below the dura at the following positions relative to the bregma: -1.5 mm anterior–posterior coordinates and 2.5 mm (AAV1.CAMK2.NES-WHaloCaMP1a-EGFP) or 4 mm (AAV1.CAMK2.NES-iGECI-EGFP) in the mediolateral coordinates. A glass window made of a single coverslip (Fisher Scientific, no. 1.5) was embedded in the craniotomy and sealed in place with dental acrylic. A titanium headpost was then attached to the skull with cyanoacrylate glue and dental acrylic. Mice were r.o. injected with 200 nmol JF₆₆₉-HaloTag ligand 24 h before the imaging session. No exogenous biliverdin was supplied for imaging.

Mice were imaged on a custom-built upright microscope as previously described⁶² with modifications. For the excitation source, we used a four-wavelength LED (Thorlabs, LED4D067). To excite WHaloCaMP1a₆₆₉ and iGECI, we used the 625-nm LED, and to image the EGFP expression marker, we used the LED at 470 nm. We used an imaging dichroic beam splitter with edge at 660 nm (FF660-Di02-25x36, Semrock) and a 671-nm emission filter (LP02-671RU-25, Semrock) to clean up fluorescence signal before camera detection. For green fluorescence imaging, we used a Thorlabs GFP filter set (MDF-GFP). Fluorescence signals were imaged using an InGaAs camera (Ninox 640 II, Raptor Photonics). Images were acquired using μManager, an open-source microscopy software⁶³. To obtain an overview image of the cranial window, we used a ×4 objective (Nikon ×4 Plan Fluor, 0.13 NA and working distance of 17.2 mm). For depth experiments and functional imaging, we used a ×10 objective (Nikon ×10 Plan Fluor, 0.3 NA and working distance of 3.5 mm). For the functional whisker-stimulation experiments, images were acquired at the focal plane. Images were acquired in a 0.11-s period for 1,727 frames. We conducted the whisker air puff stimulation using a Picospritzer III system (Parker Hannifin) with 30 psi of air pressure and a duration of 50 ms.

Stimulation was controlled using the MATLAB-based waveform generator WaveSurfer to elicit a pulse every 30 s. The pulse was delivered in a square pulse train for six consecutive trials, with a 10-s delay for the first trial.

For whisker-stimulation experiments, no ROI was chosen, and we used the whole field of view for analysis. We calculated $\Delta F/F_0 = (F - F_0)/F_0$, where F is the instantaneous fluorescence signal and F_0 is the average fluorescence in the 6-s interval before the onset of the air puff stimulus.

Zebrafish larvae

All zebrafish experiments were conducted in accordance with animal research guidelines from the National Institutes of Health and were approved by the Institutional Animal Care and Use Committee and the Institutional Biosafety Committee of Janelia Research Campus. Larvae were reared using standard protocols in 14:10 light–dark cycles at 28.5 °C.

To generate WHaloCaMP1a lines, NES-WHaloCaMP1a or NES-WHaloCaMP1a-EGFP were cloned into Tol2 vectors with the *elavl3*

pan-neuronal promoter. The plasmid was injected into one to two cell embryos from *casper* background zebrafish with mRNA encoding the Tol2 transposon. Potential founders were selected either by screening with the JF₅₂₂-HaloTag ligand or based on EGFP expression. Potential founders were then screened by outcrossing to *casper* and selecting progeny (F₁ generation) that expressed WHaloCaMP1a in the central nervous system. Experiments were performed on larvae at 4–5 dpf produced from crosses with *casper*, from in-crosses or from crossing with other lines for multicolor experiments. For three-color multiplexed functional imaging, we crossed Tg(*elavl3*:NES-WHaloCaMP1a) with Tg(*actb2*:iGlucoSnFR; *acta1a*;jRGECO1a)²⁹ animals; for neuronal and astrocyte imaging, we crossed Tg(*elavl3*:NES-WHaloCaMP1a-EGFP) with Tg(*gfap*;jRGECO1b)³⁰ animals. For comparing WHaloCaMP1a₆₆₉ to jRGECO1b in the same neuronal population, we crossed Tg(*elavl3*:NES-WHaloCaMP1a-EGFP) with Tg(*elavl3*;jRGECO1b)²⁸ animals.

Dye delivery to zebrafish larvae

Dye-ligands were delivered to the central nervous system of zebrafish larvae by adding the dye-HaloTag ligand (final concentration of 4 μM from a 2-mM stock in DMSO) to the system water for 2 h. The larvae were then washed 2× for 1 h with fresh system water before mounting for whole-brain imaging.

Whole-brain light-sheet imaging with SiMView

Whole-brain imaging was performed on a SiMView microscope as previously described^{71,72}. Tg(*elavl3*:NES-WHaloCaMP1a-EGFP) zebrafish larvae at 5 dpf were labeled with the JF₆₆₉-HaloTag ligand, as described above. The fish were screened for EGFP fluorescence, and EGFP-positive fish were paralyzed in a drop of 1 mg ml⁻¹ α-bungarotoxin solution (Invitrogen) in system water for 30 s before recovering in system water for 30 min. Zebrafish were placed in 2% agarose in system water and positioned in a custom-designed glass capillary (outer diameter of 2 mm, 20 mm long; Hilgenberg), which was mounted in an imaging chamber filled with system water. Fluorescence light-sheet imaging of WHaloCaMP1a₆₆₉ was performed with Nikon ×16, 0.8-NA water-dipping objectives and a Hamamatsu ORCA-Fusion BT camera. A 685-nm laser (1.6 mW cm⁻² at the sample) was used to excite WHaloCaMP1a₆₆₉, and light was collected through a 795/188-nm detection filter (Semrock). Volumetric imaging was performed with an exposure time of 5 ms at a step size of 4 μm across a 160-μm-deep volume, resulting in a volume imaging rate of four image stacks per second. Image analysis was performed as previously described⁷¹, using a custom-written pipeline in MATLAB (Mathworks). After analysis, WHaloCaMP1a₆₆₉ activity was visualized by creating a multichannel composite image of the ΔF/F time series images, which were superimposed on a static anatomical reference image. The anatomical reference image was generated by computing a projection of the ΔF/F images along the z and time axes and applying a CLAHE filter with a block size of 15, 255 bins and a maximum gradient of 4.

Multiplexed light-sheet imaging of far-red, red and green fluorescence in zebrafish larvae

Multiplexed light-sheet single-plane functional imaging was performed on a Zeiss Lightsheet Z.1 microscope with two pco.edge 5.5 sCMOS cameras. For single-cell resolution imaging of neuronal and astrocyte activity, fish were paralyzed in a drop of 1 mg ml⁻¹ α-bungarotoxin solution (Invitrogen) in system water for 30 s before recovering in system water for 5 min. This paralysation was not performed for three-color multiplexed imaging of Tg(*elavl3*:NES-WHaloCaMP1a) × Tg(*actb2*:iGluco SnFR; *acta1a*;jRGECO1a) animals to retain the muscle Ca²⁺ transients. Fish were mounted in 2% low melting agarose in system water in a glass capillary, and the solidified agarose extruded into an imaging chamber filled with system water for imaging. For imaging with 4-AP, a solution of 8 mM was prepared in system water, which was diluted

into the imaging chamber before imaging. The final concentration of 4-AP was 500–700 nM.

Images were acquired using an Objective W Plan-Apochromat ×10, 0.5 M27 75-mm illumination objective and two ×5, 0.1-NA objectives (with a correction ring) for side illumination. As we saw artifacts on dual-side illumination, only one side of illumination was used during acquisition. Pivot scan was always on during acquisition. Before each imaging session, the cameras were manually aligned and the light sheet was corrected using the correction rings on the ×5 illumination objectives. Single-plane light-sheet imaging was performed with 488 nm, and 561-nm and 638-nm excitation laser lines and a laser-blocking filter (Filter Module LBF 405/488/561/638) were used in the excitation light path. Exposure time was 234.69 ms.

For three-color functional imaging of Tg(*elavl3*:NES-WHaloCaMP1a) × Tg(*actb2*:iGlucoSnFR; *acta1a*;jRGECO1a) animals, two tracks were used with a filter change between the track acquisitions. This filter change decreased the imaging to 5 s per frame. In track 1, 488-nm and 638-nm excitation was used with a 560-nm beam splitter. The emission filter (505–545 nm) was in front of camera 1, and a longpass 660-nm filter was in front of camera 2. In track 2, 561-nm excitation light was used with a 640-nm beam splitter and a 575–615-nm emission filter in front of camera 1. Images were acquired at 1× zoom for up to 60 min at 1,000 × 1,800 pixels. Images were registered using Suite2p³¹ before ΔF/F₀ values of ROI determined in Fiji⁶⁰ were calculated using a rolling average of 250 frames with the lowest 0.1 quantile used for F₀.

For dual-color imaging with Tg(*elavl3*:NES-WHaloCaMP1a-EGFP) × Tg(*gfap*;jRGECO1b) and Tg(*elavl3*:NES-WHaloCaMP1a-EGFP) × Tg(*elavl3*;jRGECO1b) animals, anatomical images were first acquired, with single-fluorophore excitation of EGFP, 488-nm excitation, 560-nm beam splitter, 505–545-nm emission filter; jRGECO1b, 561-nm excitation, 640-nm beam splitter, 575–615-nm emission filter; WHaloCaMP1a₆₆₉, 638-nm excitation, 560-nm beam splitter, longpass 660-nm emission filter. Functional imaging was performed with simultaneous 561-nm and 638-nm excitation light, a 560-nm beam splitter and a 575–615-nm emission filter in front of camera 1 and a longpass 660-nm emission filter in front of camera 2. The 561-nm light was reduced to the lowest amount to limit bleedthrough of the jRGECO1b signal to the far-red emission channel. Images were acquired at 2.5× zoom, a pixel size of 1,960 × 1,960, 354.4 μm × 354.4 μm and 0.18 μm per pixel. Time series of 1,500 frames were collected. Time series were concatenated together when longer analysis was desired. Images were downsampled for analysis.

Image analysis of single-plane light-sheet neuronal and astrocyte imaging

For analysis of dual-color functional imaging of WHaloCaMP1a₆₆₉ in neurons and jRGECO1b in astrocytes, a combination of Fiji⁶⁰, Suite2p³¹, Cellpose³² and Rastermap³³ was used. The two channels were analyzed separately. First, Suite2p was used for registration of the images, and cell segmentation was performed using Cellpose seeding with a manually determined diameter. Suite2p was then used to extract traces from the segmented cells. The ΔF/F₀ was calculated using a rolling average of 100 frames (for *elavl3*-jRGECO1b acquisitions) or 200 frames (for *gfap*-jRGECO1b acquisitions), with F₀ calculated from the lowest 0.1 quantile. Fluorescent traces were clustered with Rastermap before being presented as heatmaps.

Fluorescence lifetime imaging microscopy

FLIM was performed on a STELLARIS 8 FALCON microscope (Leica Microsystems) with a white light laser with tunable excitation wavelengths from 440 to 790 nm operating at 80 MHz. For full lifetime decay calculations, the microscope was set to operate at 40 MHz. A ×20 water-immersion objective (Leica, HC PL IRAPO, NA = 0.75) or a ×25 water-immersion objective (Leica, HC FLUOTAR L, NA = 0.95) was used. HyD photon-counting detectors were used.

FLIM of purified protein

To generate a calibration curve of lifetime versus Ca^{2+} concentration in purified protein, WHaloCaMP1a was labeled with a dye-ligand and diluted into solutions made by mixing different proportions of concentrations made from Calcium Calibration Buffer Kit #1 (Invitrogen). A small drop was placed on a microscope slide, and a double adhesive divider was placed on the slide before it was covered with a coverslip (#1.5). For WHaloCaMP1a₄₉₄, excitation was 488 nm, and emission collected on a HyDX2 was set to 500–575 nm. For WHaloCaMP₅₅₂, excitation was 561 nm, and emission collected on a HyDS3 was set to 575–650 nm. For WHaloCaMP₆₆₉, excitation was 671 nm, and emission collected on a HyDX4 was set to 680–780 nm. For WHaloCaMP₇₂₂, excitation was 730 nm, and emission collected on a HyDR5 was set to 745–850 nm. For iGECI imaging, excitation was 638 nm, and emission collected on a HyDX4 was set to 650–700 nm.

FLIM in tissue cultured cells

The Janelia Cell Culture Facility performed tissue culture and regular *Mycoplasma* testing. HeLa cells (CCL-2) were purchased from ATCC. No authentication of the cell line was performed. Cells were cultured in DMEM medium (phenol red free, Life Technologies) supplemented with 10% (vol/vol) FBS (Life Technologies) and 1 mM GlutaMAX (Life Technologies). Cells were cultured at 37 °C in a humidified 5% (vol/vol) CO_2 environment. Cells were transiently transfected by nucleofection (Lonza) 24 h before imaging and plated in 35-mm dishes (MatTek, #1.5 coverslip). Before imaging, cells were labeled with 50 nM JF₆₆₉-HaloTag ligand in growth medium before being washed 2× with imaging buffer containing 145 mM NaCl, 2.5 mM KCl, 10 mM glucose, 10 mM HEPES, pH 7.4, 2 mM CaCl_2 and 1 mM MgCl_2 for histamine stimulation experiments or Hanks' Balanced Salt Solution with no Ca^{2+} , no magnesium and no phenol red (Thermo Fisher Scientific, 14175095) for Ca^{2+} titration experiments. Images were collected at 1,600 × 1,600 pixels, with the pinhole set to 1 AU and 2× zoom. Images were collected every 5 s for 10 min.

For cellular Ca^{2+} titration experiments, Ca^{2+} -free Hanks' Balanced Salt Solution was replaced with solutions with Ca^{2+} free concentrations made from Calcium Calibration Buffer Kit #1 (Invitrogen) with 0 mM and 10 mM CaEGTA and equilibrated for 10 min at 37 °C. Digitonin (Promega, G944A) was then used to permeabilize the cells. The digitonin stock was diluted to 2 mg ml⁻¹ in buffer, and 1 µl was added to the 2-ml volume in the imaging dish immediately before acquisition, giving a final concentration of 1 µM.

For histamine stimulation experiments, histamine was diluted in imaging buffer to a 100-mM stock solution. This was further diluted by adding 20 µl to the 2 ml of imaging buffer on the cells to give a final concentration of 1 µM.

FLIM of neurons in zebrafish larvae

Zebrafish larvae (*Tg(elavl3:NES-WHaloCaMP1a-EGFP*, 4–5 dpf) were labeled and paralyzed as described above. The fish were then mounted, with the brain closest to the coverslip, in 2% low melting agarose in a 35-mm dish (MatTek, #1.5 coverslip). The fish were imaged in system water with 6× zoom, the pinhole set to 1 AU and 512 × 512 pixels. The imaging rate was one frame per second.

FLIM image analysis

Fluorescence lifetime fitting was performed in LAS X FLIM software. A spatial binning of 2 was performed, and each time point was split in the software. A three-component fit was used to fit the fluorescence lifetime. The amplitude-weighted fluorescence lifetime for the whole image is reported for WHaloCaMP1a labeled with different dye-ligands and imaged at 40 MHz. For quantifying concentrations of Ca^{2+} in HeLa cells and neurons of zebrafish larvae, each pixel in the image was fit to a decay curve. The fit was performed on images that had a threshold of 20–50 counts for each pixel. The image was then exported to a TIFF

file with a scaling factor of 0.001 on the lifetime and analyzed in Fiji⁶⁰. A calibration curve from the purified protein or digitonin-lysed cells was fit using a four-parameter dose-response curve (variable slope) using GraphPad Prism software. a is the value of fluorescence at the bottom of the curve, b is the value of fluorescence at the top of the curve, EC_{50} is the concentration of agonist that gives a response halfway between the bottom and the top, and h is the Hill or cooperative coefficient.

$$y = a + \frac{x^h \times (b-a)}{x^h + \text{EC}_{50}^h} \quad x = \text{EC}_{50} \left(\frac{a-y}{y-b} \right)^{\left(\frac{1}{h} \right)}$$

To calculate the cellular Ca^{2+} concentration, the equation was rearranged, and a value of $x = [\text{Ca}^{2+}]$ was calculated for each measured value of y (lifetime (ns)) for an ROI in a time series. The intensity channel was also exported from LAS X FLIM software, and the $\Delta F/F$ was calculated from the first quartile for the time series. For visualization purposes for the lifetime time series, a Gaussian filter of 0.8 was used. All quantitative analysis was performed on the raw exported images before any image processing.

Reporting summary

Further information on research design is available in the Nature Portfolio Reporting Summary linked to this article.

Data availability

The data used to generate the figures in this study are available from the figshare repository: <https://doi.org/10.25378/janelia.25934782> (ref. 73). The structure of HaloTag7 bound to JF₆₆₉ has been deposited in the Protein Data Bank (PDB 8SW8). Sequences have been deposited to GenBank under accession codes PQ141081 (WHaloCaMP1a), PQ141082 (WHaloCaMP1b) and PQ141083 (WHaloCaMP_eNOSpep). DNA plasmids encoding WHaloCaMP used in this work are available from Addgene as follows: 205303, pRSET-WHaloCaMP1a-EGFP; 205304, pRSET-WHaloCaMP1a; 205305, pRSET-WHaloCaMP1b-EGFP; 205306, pRSET-WHaloCaMP-eNOSpep-EGFP; 205307, pAAV-synapsin-WHaloCaMP1a-EGFP; 205308, pAAV-synapsin-WHaloCaMP1a; 205309, pAAV-CaMKII-WHaloCaMP1a-EGFP; 205310, pAAV-CaMKII-WHaloCaMP1a; 205311, pTol2-elavl3-WHaloCaMP1a-EGFP; 205312, pTol2-elavl3-WHaloCaMP1a; 205313, pCAG-WHaloCaMP1a-EGFP; 205314, p10xUAS-WHaloCaMP1a-EGFP.

Code availability

The MATLAB programs for ScanImage for data acquisition and analysis for multiplexed imaging in acute brain slices with WHaloCaMP1a₆₆₉ and FLIM-AKAR are available at https://github.com/YaoChenLabWashU/2pFLIM_acquisition. MATLAB 2012b was used.

References

45. Studier, F. W. Protein production by auto-induction in high-density shaking cultures. *Protein Expr. Purif.* **41**, 207–234 (2005).
46. Winter, G. *xia2*: an expert system for macromolecular crystallography data reduction. *J. Appl. Crystallogr.* **43**, 186–190 (2010).
47. Winter, G. et al. DIALS: implementation and evaluation of a new integration package. *Acta Crystallogr. D* **74**, 85–97 (2018).
48. Winn, M. D. et al. Overview of the CCP4 suite and current developments. *Acta Crystallogr. D* **67**, 235–242 (2011).
49. McCoy, A. J. et al. Phaser crystallographic software. *J. Appl. Crystallogr.* **40**, 658–674 (2007).
50. Murshudov, G. N., Vagin, A. A. & Dodson, E. J. Refinement of macromolecular structures by the maximum-likelihood method. *Acta Crystallogr. D* **53**, 240–255 (1997).
51. Emsley, P., Lohkamp, B., Scott, W. G. & Cowtan, K. Features and development of Coot. *Acta Crystallogr. D* **66**, 486–501 (2010).

52. Kille, S. et al. Reducing codon redundancy and screening effort of combinatorial protein libraries created by saturation mutagenesis. *ACS Synth. Biol.* **2**, 83–92 (2013).
53. Mütze, J. et al. Excitation spectra and brightness optimization of two-photon excited probes. *Biophys. J.* **102**, 934–944 (2012).
54. Xu, C. & Webb, W. W. Measurement of two-photon excitation cross sections of molecular fluorophores with data from 690 to 1050 nm. *J. Opt. Soc. Am. B* **13**, 481–491 (1996).
55. Makarov, N. S., Drobizhev, M. & Rebane, A. Two-photon absorption standards in the 550–1600 nm excitation wavelength range. *Opt. Express* **16**, 4029–4047 (2008).
56. Suzuki, K. et al. Reevaluation of absolute luminescence quantum yields of standard solutions using a spectrometer with an integrating sphere and a back-thinned CCD detector. *Phys. Chem. Chem. Phys.* **11**, 9850–9860 (2009).
57. Tsien, R. & Pozzan, T. in *Methods in Enzymology* Vol. 172 (Academic Press, 1989).
58. Abdelfattah, A. S. et al. Bright and photostable chemogenetic indicators for extended in vivo voltage imaging. *Science* **365**, 699–704 (2019).
59. Kremers, G.-J., Hazelwood, K. L., Murphy, C. S., Davidson, M. W. & Piston, D. W. Photoconversion in orange and red fluorescent proteins. *Nat. Methods* **6**, 355–358 (2009).
60. Schindelin, J. et al. Fiji: an open-source platform for biological-image analysis. *Nat. Methods* **9**, 676–682 (2012).
61. Wardill, T. J. et al. A neuron-based screening platform for optimizing genetically-encoded calcium indicators. *PLoS ONE* **8**, e77728 (2013).
62. Bulumulla, C. et al. Visualizing synaptic dopamine efflux with a 2D composite nanofilm. *eLife* **11**, e78773 (2022).
63. Edelstein, A. D. et al. Advanced methods of microscope control using μManager software. *J. Biol. Methods* **1**, e10 (2014).
64. Gorski, J. A. et al. Cortical excitatory neurons and glia, but not GABAergic neurons, are produced in the *Emx1*-expressing lineage. *J. Neurosci.* **22**, 6309–6314 (2002).
65. Pologruto, T. A., Sabatini, B. L. & Svoboda, K. ScanImage: flexible software for operating laser scanning microscopes. *Biomed. Eng. Online* **2**, 13 (2003).
66. Mohr, M. A. et al. jYCaMP: an optimized calcium indicator for two-photon imaging at fiber laser wavelengths. *Nat. Methods* **17**, 694–697 (2020).
67. Pelli, D. G. The VideoToolbox software for visual psychophysics: transforming numbers into movies. *Spat. Vis.* **10**, 437–442 (1997).
68. Sun, W., Tan, Z., Mensh, B. D. & Ji, N. Thalamus provides layer 4 of primary visual cortex with orientation- and direction-tuned inputs. *Nat. Neurosci.* **19**, 308–315 (2016).
69. Chen, T.-W. et al. Ultrasensitive fluorescent proteins for imaging neuronal activity. *Nature* **499**, 295–300 (2013).
70. Ohki, K., Chung, S., Ch'ng, Y. H., Kara, P. & Reid, R. C. Functional imaging with cellular resolution reveals precise micro-architecture in visual cortex. *Nature* **433**, 597–603 (2005).
71. Lemon, W. C. et al. Whole-central nervous system functional imaging in larval *Drosophila*. *Nat. Commun.* **6**, 7924 (2015).
72. Wan, Y. et al. Single-cell reconstruction of emerging population activity in an entire developing circuit. *Cell* **179**, 355–372 (2019).
73. Schreiter, E. & Farrants, H. WHaloCaMP data. figshare <https://doi.org/10.25378/janelia.25934782> (2024).

Acknowledgements

We thank the Vivarium, Cell Culture, Imaging, Media Prep, Molecular Biology, Virus Production and Fly Facilities at Janelia Research Campus for assistance. We especially thank D. Walpita, J. Cox, D. Alcor, M. DeSantis, J. Rouchard and S. Dilisio. We thank A.G. Tebo for critical comments on the paper and help with collecting X-ray diffraction data, B. Mohar for guidance on dye-ligand choices for use in living

animals and S.-H. Sheu for helpful comments on FLIM. We thank the Ahrens laboratory at Janelia Research Campus for use of animals and useful comments on zebrafish larva experiments. This work was supported by the Howard Hughes Medical Institute. The contributions of C.M.H. and Y.C. are supported by the US National Institute of Neurological Disorders and Stroke (R01 NS119821 to Y.C.) and the Mathers Foundation (28323 to Y.C.). M.S.F. acknowledges funding and resources from the Max Planck Institute for Medical Research, Heidelberg, Germany. Y.L. was supported by the Maryland Stem Cell Research Fund (2022-MSCRFL-5893 to Y.L.). The Berkeley Center for Structural Biology is supported in part by the Howard Hughes Medical Institute. The Advanced Light Source is a Department of Energy Office of Science User Facility under contract no. DE-AC02-05CH11231.

Author contributions

H.F. and E.R.S. conceived the project and wrote the paper with input from all authors. H.F. contributed to X-ray crystallography, designed, screened and characterized all WHaloCaMP variants in vitro and in neuronal cultures, performed and analyzed functional imaging in zebrafish larvae and in mice and performed all FLIM experiments with WHaloCaMP. E.R.S. contributed to WHaloCaMP design and X-ray crystallography. Y.S. performed and analyzed experiments in *Drosophila*, and G.C.T. oversaw these experiments. W.C.L. and P.J.K. performed and analyzed data from SIMView light-sheet microscopy, and P.J.K. oversaw these experiments. C.M.H. performed and analyzed experiments in acute brain slices, and Y.C. contributed to the analysis and oversaw these experiments. D.Z. contributed to one-photon imaging in the mouse cortex, and A.G.B. oversaw these experiments. S.Y. contributed to optogenetic and electrophysiology experiments. R.P. characterized WHaloCaMPs under multiphoton excitation. G.Q. performed surgeries for functional imaging of the mouse cortex, and Y.L. performed and analyzed functional imaging of the mouse cortex and oversaw these experiments. M.S.F. contributed to WHaloCaMP design. S.E.P., J.B.G. and L.D.L. synthesized and developed JF dyes and determined their in vitro properties, and L.D.L. oversaw this work. T.L.H. and F.T. built and developed an assay for functional imaging in the mouse cortex. C.S. contributed analysis scripts for functional imaging of zebrafish larvae and mice. A.G.B. contributed to neuronal imaging of WHaloCaMP₇₂₂ and one-photon imaging in the mouse cortex. E.R.S. directed the project.

Competing interests

H.F. and E.R.S. have filed patent applications on tryptophan-containing chemogenetic fluorescent indicators. L.D.L. and J.B.G. have filed patents and patent applications on fluorinated and azetidine-containing rhodamines. The other authors declare no competing interests.

Additional information

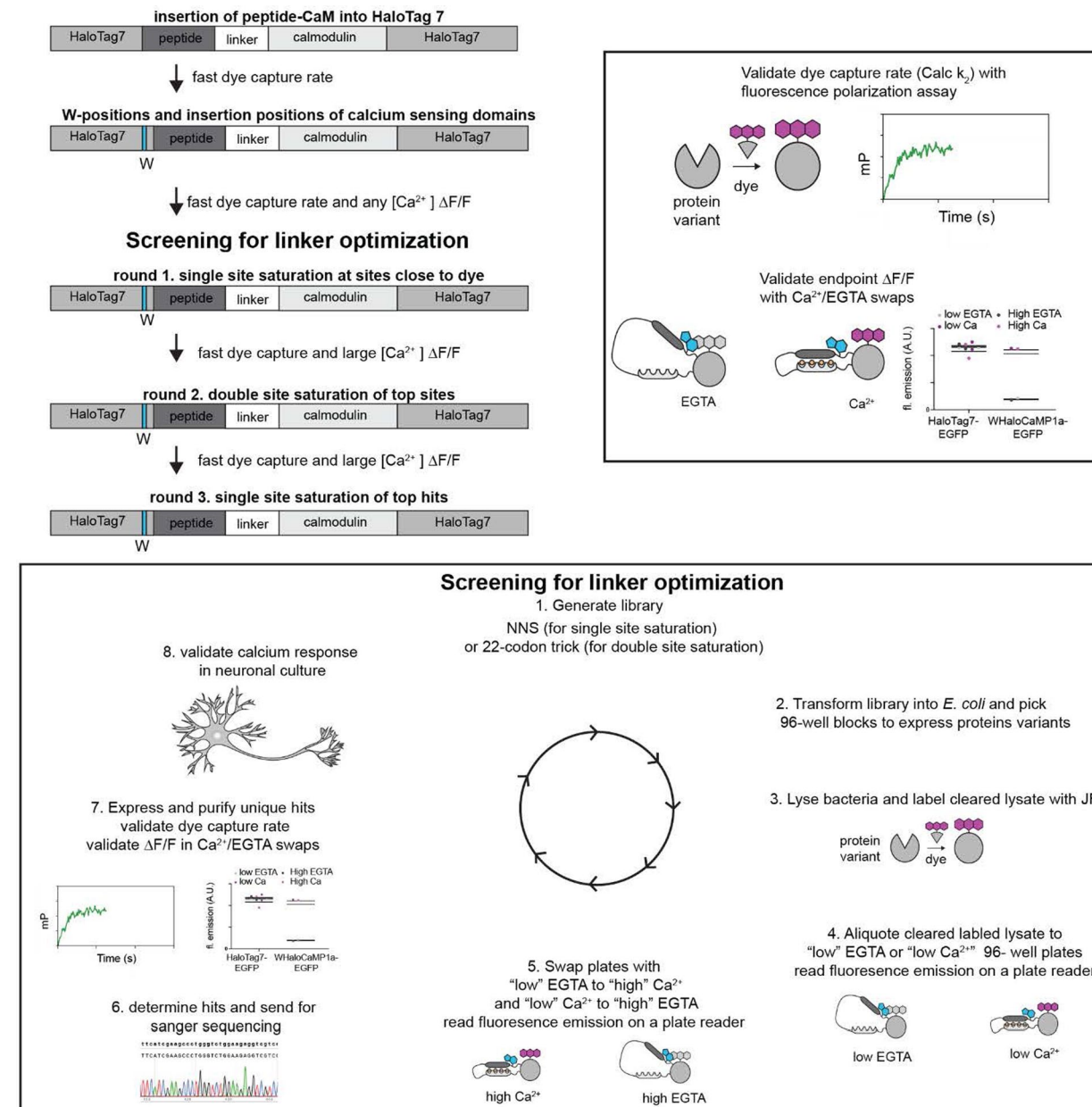
Extended data is available for this paper at <https://doi.org/10.1038/s41592-024-02411-6>.

Supplementary information The online version contains supplementary material available at <https://doi.org/10.1038/s41592-024-02411-6>.

Correspondence and requests for materials should be addressed to Helen Farrants or Eric R. Schreiter.

Peer review information *Nature Methods* thanks Michael Häusser and the other, anonymous, reviewer(s) for their contribution to the peer review of this work. Primary Handling Editor: Nina Vogt, in collaboration with the *Nature Methods* team.

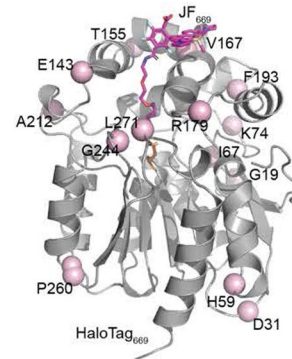
Reprints and permissions information is available at www.nature.com/reprints.



Extended Data Fig. 1 | Engineering strategy for WHaloCaMPs. Engineering of WHaloCaMPs was performed in several consecutive steps. First, insertion sites of Calmodulin (CaM) and a CaM-binding peptide were explored. Insertion sites with high dye capture rate were moved forward to explore rational tryptophan mutations together with insertions. The variants with fastest dye capture

rate and any fluorescence modulation upon calcium addition were moved forward to targeted directed evolution through single or double site saturation mutagenesis. After each round, Ca^{2+} indicator performance was validated in cultured neurons in a field stimulation assay.

HaloTag7	HaloTag7
HaloCaMP1a	MLCK-peptide L1 HaloTag7 C-term (GGT/S) ₆ HaloTag7 N-term L2 calmodulin
HaloCaMP1b	CKK-peptide L1 HaloTag7 C-term (GGT/S) ₆ HaloTag7 N-term L2 calmodulin
Insertion variants	HaloTag7 N-term L1 MLCK-peptide (GGS) ₄ calmodulin L2 HaloTag7 C-term
	HaloTag7 N-term L1 CKK-peptide (GGS) ₄ calmodulin L2 HaloTag7 C-term
MLCK-peptide	ARRKWQKTGHAVRAIGRLSS
CKK-peptide	VRVIPRLDTLILVKAMGHRKRGFGNPFR



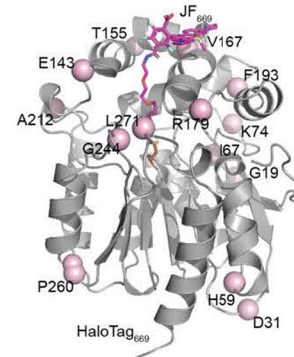
EGTA Calc k ₂ (M ⁻¹ s ⁻¹)		Ca ²⁺ Calc k ₂ (M ⁻¹ s ⁻¹)	
HaloTag7	Over 10 ⁶	Over 10 ⁶	Over 10 ⁶
HaloCaMP1a	1 × 10 ⁵ ± 1 × 10 ⁴		Over 10 ⁶
HaloCaMP1b	1 × 10 ⁵ ± 7 × 10 ³		8 × 10 ⁴ ± 9 × 10 ³

Insertion at	L1	Peptide-(GGS) ₄ -CaM /CaM-(GGS) ₄ -peptide	L2	Calc k ₂ (M ⁻¹ s ⁻¹) EGTA	Calc k ₂ (M ⁻¹ s ⁻¹) Ca ²⁺
G19	-	MLCK-(GGS) ₄ -CaM	-	Over 10 ⁶	Over 10 ⁶
D31	-	MLCK-(GGS) ₄ -CaM	-	Over 10 ⁶	Over 10 ⁶
H59	-	MLCK-(GGS) ₄ -CaM	-	Over 10 ⁶	Not measured
I67	-	MLCK-(GGS) ₄ -CaM	-	6 × 10 ³ ± 3 × 10 ³	Below 10 ³
K74	-	MLCK-(GGS) ₄ -CaM	-	Over 10 ⁶	Over 10 ⁶
E143	GGS	MLCK-(GGS) ₄ -CaM	GGS	1 × 10 ⁵ ± 1 × 10 ⁴	1 × 10 ⁵ ± 1 × 10 ⁴
	-	MLCK-(GGS) ₄ -CaM	-	1 × 10 ⁵ ± 2 × 10 ⁴	1 × 10 ⁵ ± 2 × 10 ⁴
T155	Delta T155	MLCK-(GGS) ₄ -CaM	Delta D156	Over 10 ⁶	Over 10 ⁶
	Delta T154 Delta T155	MLCK-(GGS) ₄ -CaM	Delta D156 Delta V157	Over 10 ⁶	9 × 10 ⁴ ± 9 × 10 ³
	Delta R153 Delta T154 Delta T155	MLCK-(GGS) ₄ -CaM	Delta D156 Delta V157 Delta G158	Below 10 ³	Below 10 ³
	GGS	CKK-(GGS) ₄ -CaM	GGS	Over 10 ⁶	Over 10 ⁶
	-	CKK-(GGS) ₄ -CaM	-	Over 10 ⁶	4 × 10 ⁵ ± 1 × 10 ⁵
	Delta T155	CKK-(GGS) ₄ -CaM	Delta D156	Over 10 ⁶	3 × 10 ⁵ ± 1 × 10 ⁴
	Delta T154 Delta T155	CKK-(GGS) ₄ -CaM	Delta D156 Delta V157	1 × 10 ⁴ ± 8 × 10 ³	7 × 10 ⁴ ± 4 × 10 ³
V167	-	MLCK-(GGS) ₄ -CaM	-	5 × 10 ³	Below 10 ³
R179	-	MLCK-(GGS) ₄ -CaM	-	Over 10 ⁶	8 × 10 ⁴ ± 1 × 10 ⁴
F193	-	MLCK-(GGS) ₄ -CaM	-	Over 10 ⁶	Over 10 ⁶
A212	-	MLCK-(GGS) ₄ -CaM	-	3 × 10 ⁵	5 × 10 ⁵
G244	-	MLCK-(GGS) ₄ -CaM	-	Below 10 ³	Below 10 ³
P260	-	MLCK-(GGS) ₄ -CaM	-	3 × 10 ⁵ ± 1 × 10 ⁵	3 × 10 ⁵ ± 3 × 10 ⁴
L271	-	MLCK-(GGS) ₄ -CaM	-	6 × 10 ³	Below 10 ³

Extended Data Fig. 2 | Insertion of Ca²⁺ sensing domains into HaloTag7. 1D schematic of the topology of the insertion variants of CaM and CaM-binding peptide into HaloTag7 in comparison to HaloCaMP. The crystal structure of HaloTag7 bound to JF₆₆₉-HaloTag ligand is shown, highlighting the insertion

positions. Bottom two tables report the measured dye capture rate with JF₅₄₉-HaloTag ligand and the indicated protein. The insertion position (R179) which led to WHaloCaMP1a is highlighted in magenta.

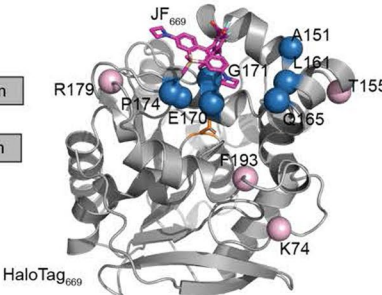
HaloTag7	HaloTag7
MLCK-peptide	L1 HaloTag7 C-term (GGT/S) ₆ HaloTag7 N-term L2 calmodulin
CKK-peptide	L1 HaloTag7 C-term (GGT/S) ₆ HaloTag7 N-term L2 calmodulin



Insertion variants	HaloTag7 N-term L1 MLCK-peptide (GGS) ₄ calmodulin L2 HaloTag7 C-term
	HaloTag7 N-term L1 CKK-peptide (GGS) ₄ calmodulin L2 HaloTag7 C-term

MLCK-peptide
CKK-peptide
ARRKWQKTGHAVRAIGRLSS
VRVIPRLDTLILVKAMGHRKRGNPFR

HaloTag7	HaloTag7
Insertion variants	HaloTag7 N-term L1 MLCK-peptide (GGS) ₄ calmodulin L2 HaloTag7 C-term
	HaloTag7 N-term L1 MLCK-peptide (GGS) ₄ calmodulin L2 HaloTag7 C-term *

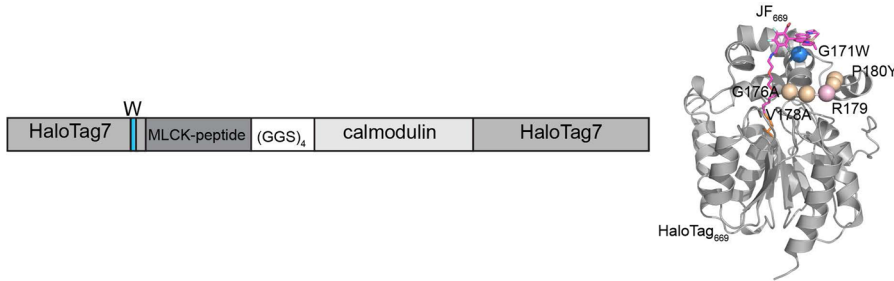


Protein	W mutation	Calc k ₂ (M ⁻¹ s ⁻¹) EGTA	ΔF/F ₀
HaloTag7	G171W	Over 10 ⁶	0.0 ± 0.1
HaloTag7	A151W	Over 10 ⁶	0.0 ± 0.1

Insertion at	Insertion of	W mutation	Calc k ₂ (M ⁻¹ s ⁻¹) EGTA	ΔF/F ₀
K74	MLCK -(GGS) ₄ -CaM	G171W	Over 10 ⁶	0.0 ± 0.1
T155	MLCK -(GGS) ₄ -CaM	G171W	Over 10 ⁶	0.0 ± 0.0
	Delta T155 MLCK -(GGS) ₄ -CaM Delta D156	A151W	4 × 10 ⁵	0.2 ± 0.1
	Delta T154 Delta T155 MLCK -(GGS) ₄ -CaM Delta D156 Delta V157	A151W	2 × 10 ⁵	-0.3 ± 0.1
	Delta T155 MLCK -(GGS) ₄ -CaM Delta D156	L161W	6 × 10 ⁴ ± 7 × 10 ³	0.2 ± 0.1
	Delta T155 MLCK -(GGS) ₄ -CaM Delta D156	Q165W	3 × 10 ⁵ ± 1 × 10 ⁴	0.2 ± 0.1
	Delta T155 MLCK -(GGS) ₄ -CaM Delta D156	E170W	4 × 10 ³	-0.1 ± 0.2
R179	MLCK - (GGS) ₄ -CaM	P174W	2 × 10 ⁴ ± 5 × 10 ³	0.2 ± 0.1
	MLCK - (GGS) ₄ -CaM	G171W	Over 10 ⁶	0.2 ± 0.1
F193	MLCK - (GGS) ₄ -CaM	G171W	Over 10 ⁶	0.0 ± 0.2

Extended Data Fig. 3 | Tryptophan placements for WHaloCaMP development. 1D schematic of the topology of insertion variants of CaM and CaM-binding peptide into HaloTag7 (top left). Tryptophan positions are annotated with a blue star. The crystal structure of HaloTag7 bound to JF₆₆₉-HaloTag ligand is shown, highlighting the insertion positions and tryptophan placements (top right).

Bottom tables show the measured dye capture rate with JF₅₄₉-HaloTag ligand and the indicated protein, and any change in fluorescence emission ΔF/F₀ with JF₆₆₉-HaloTag ligand. The insertion position (R179), and the tryptophan placement (G171W) which led to WHaloCaMP1a is highlighted in magenta.



Round 1: single site saturations on top of insertion at site R179 with G171W
V167X, I169X, E170X, L173X, P174X, M175X, G176X, V178X, R179X, P180X, L181X, T182X

Mutation	Calc k_2 ($M^{-1} s^{-1}$) EGTA	Calc k_2 ($M^{-1} s^{-1}$) Ca^{2+}	$\Delta F/F_0$
G176V			1.2 ± 0.1
G176C			0.8 ± 0.2
V178R	$4 \times 10^5 \pm 4 \times 10^4$	$3 \times 10^4 \pm 1 \times 10^4$	2.1 ± 0.2
P180Y			1.4 ± 0.3
P180V			1.1 ± 0.2
P180I			1.3 ± 0.2
P180W	Over 10^6	$3 \times 10^4 \pm 9 \times 10^3$	1.8 ± 0.2
P180R			1.5 ± 0.2

Round 2: double site saturation of top sites of round 1
V178X, P180X

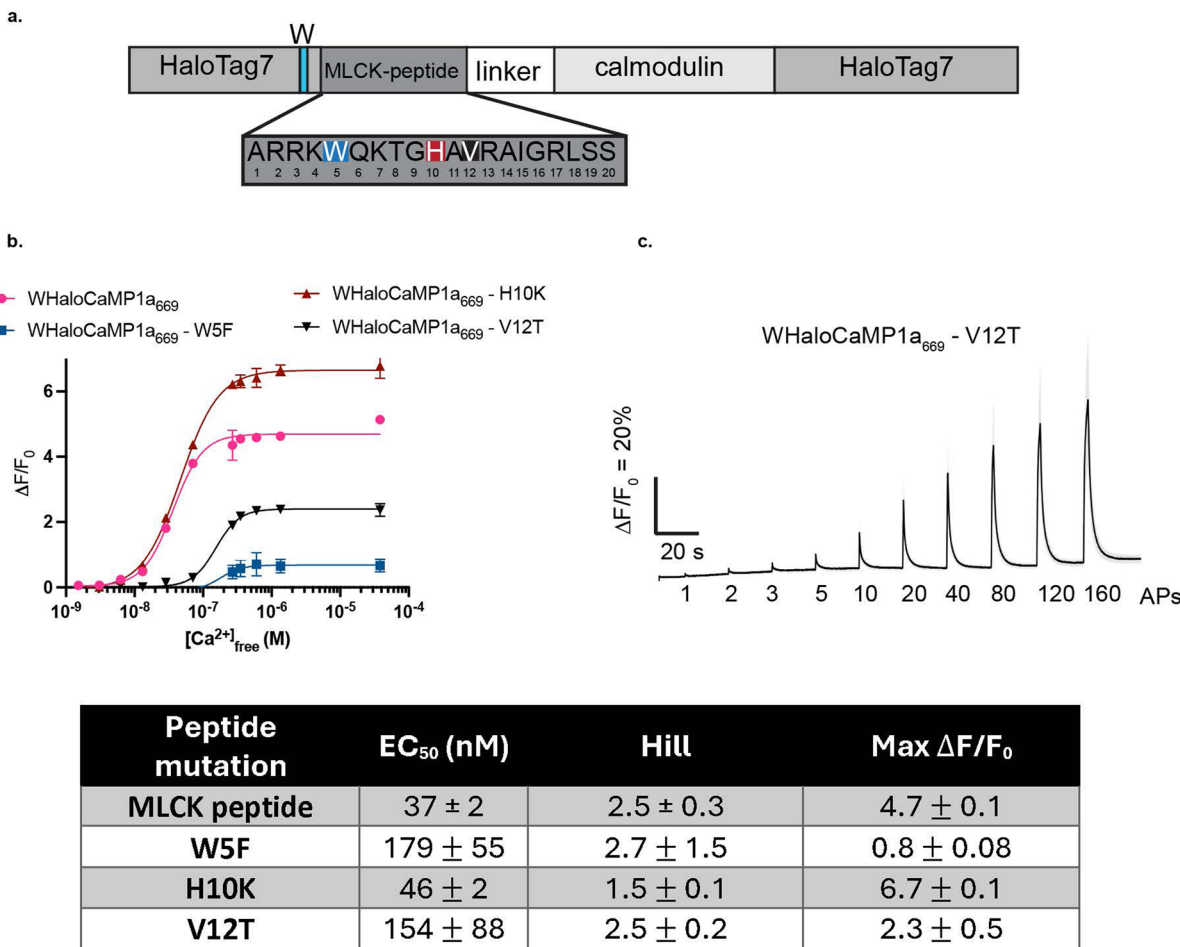
Mutation	Mutation	Calc k_2 ($M^{-1} s^{-1}$) EGTA	Calc k_2 ($M^{-1} s^{-1}$) Ca^{2+}	$\Delta F/F_0$
V178A	P180Y	Over 10^6	$8 \times 10^4 \pm 3 \times 10^4$	6.3 ± 0.0
V178A	P180V	Over 10^6	$9 \times 10^4 \pm 3 \times 10^4$	5.0 ± 0.1
V178C	P180Y	Over 10^6	$1 \times 10^5 \pm 3 \times 10^4$	5.1 ± 0.0
V178C	P180G	Over 10^6	$1 \times 10^5 \pm 4 \times 10^4$	4.5 ± 0.5
V178C	P180R	Over 10^6	$3 \times 10^5 \pm 9 \times 10^4$	4.6 ± 0.5

Round 3: single site saturation on top of hit from round 2
T148X, L161X, Q165X, I169X, E170, T172X, P174X, G176X,

Mutation	Mutation	Mutation	Calc k_2 ($M^{-1} s^{-1}$) EGTA	Calc k_2 ($M^{-1} s^{-1}$) Ca^{2+}	$\Delta F/F_0$
V178A	P180Y	G176A	Over 10^6	$2 \times 10^5 \pm 7 \times 10^4$	5.6 ± 0.8
V178A	P180Y	Q165R	$2 \times 10^5 \pm 1 \times 10^5$	$8 \times 10^3 \pm 3 \times 10^3$	5.9 ± 0.6

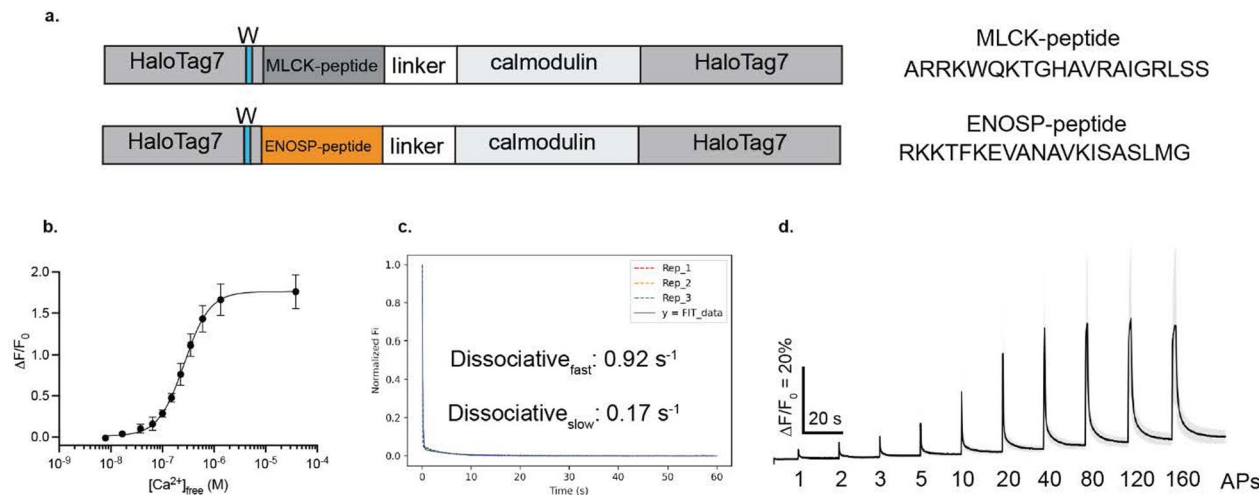
Extended Data Fig. 4 | Design of WHaloCaMP1a. ID schematic of the topology (top left) of the insertion variants of CaM and CaM-binding peptide into HaloTag7 with tryptophan position and highlighted residues on the crystal structure of HaloTag₆₆₉ (top right). Tables report top hits from sequential mutagenic library screens. First, sites close to the dye binding site were chosen for single site saturation. Double site saturation was then performed on the top two sites

from the first round of screening. A third round of single site saturation on top of the best performing variant was then performed with sites close to the dye binding site. After each round, dye capture rates of top hits were measured by fluorescence polarization using JF₅₄₉-HaloTag ligand and a calcium endpoint assay measured to validate fluorescence modulation by calcium using JF₆₆₉-HaloTag ligand. WHaloCaMP1a is highlighted in magenta.



Extended Data Fig. 5 | Reduced Ca^{2+} affinity of WHaloCaMP by mutations. **a**, Previously described mutations in the CaM-binding peptide were mapped onto WHaloCaMP1a. **b**, Ca^{2+} titrations of MLCK peptide variants (top) and values extracted from curve fits (bottom table). Titrations are plotted as the mean and s.d. of two technical replicates. **c**, Fluorescence trace (black) from

WHaloCaMP1a₆₆₉-V12T in primary neuron culture with field stimulation. Grey trace is s.e.m. F_0 was calculated 1 s before the first field stimulus. WHaloCaMP1a₆₆₉-V12T showed faster fluorescence decay in neurons compared to WHaloCaMP1a, but lower $\Delta F/F_0$ response at single AP, therefore WHaloCaMP1a₆₆₉ was used for *in vivo* demonstrations.



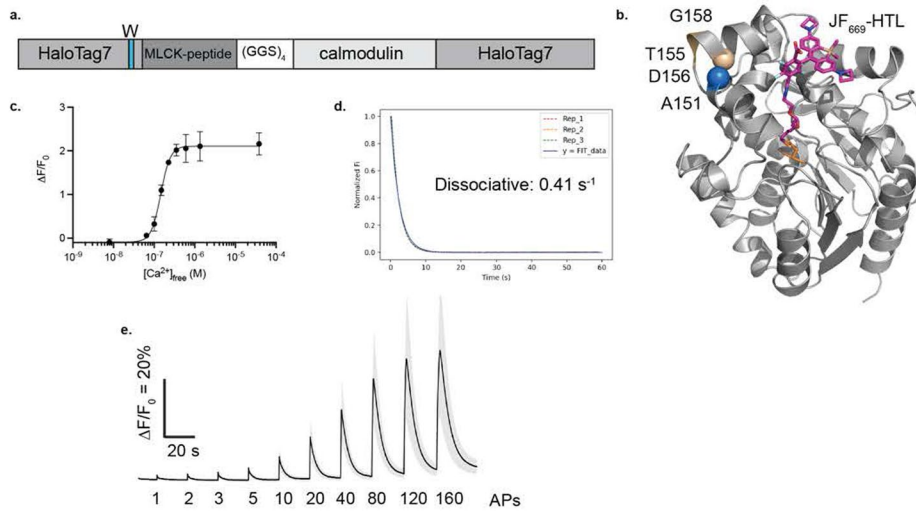
Round 1: Diversify 178X and P180X → hit V178I and P180T

Round 2: Diversify T148X, L161X, Q165X, I169X, E170X, T172X, P174X, G176X

variant	Calc $k_2 (\text{M}^{-1} \text{s}^{-1})$ EGTA	Calc $k_2 (\text{M}^{-1} \text{s}^{-1})$ Ca^{2+}	Max $\Delta F/F_0$ (endpoint)	$\text{EC}_{50} (\text{nM})$	Hill
ENOSP G171W - W quench	Over 10^6	$1 \times 10^5 \pm 3 \times 10^4$	1.5 ± 0.1	-	-
ENSP - peptide G171W - W quench V178I, P180T, G176A	Over 10^6	$4 \times 10^5 \pm 2 \times 10^5$	4.6 ± 0.4	263 ± 17	1.8 ± 0.2

Extended Data Fig. 6 | Peptide swap in WHaloCaMP1a for faster Ca^{2+} kinetics.
a. The MLCK peptide used in WHaloCaMP1a (top) was replaced with the ENOSP-peptide used in jGCaMP8 series (bottom). Two rounds of directed evolution were performed on the new scaffold: the first round was a double site saturation of sites important in the evolution of WHaloCaMP1a; the second was single site saturation on top of the top hit from the first round, which gave a variant (V178I, P180T, G176A) with fast dye capture rate, lower Ca^{2+} affinity (**b.**) titrations is plotted as the mean and s.d. of three technical replicates, and fast Ca^{2+} kinetics

measured by stopped flow (**c.**). **d.** A representative fluorescence trace from a field stimulation (black) from one run of the field stimulation assay with ~40 neuron ROIs. Grey trace is standard error of the mean (s.e.m.) of the fluorescence trace. F_0 was calculated 1s before the first field stimulus. Table reports fits from experiments in panels **b.** Even though the ENOSP variant had faster Ca^{2+} kinetics in neurons, it had lower $\Delta F/F_0$ response at single AP, therefore WHaloCaMP1a₆₆₉ was used for *in vivo* demonstrations.



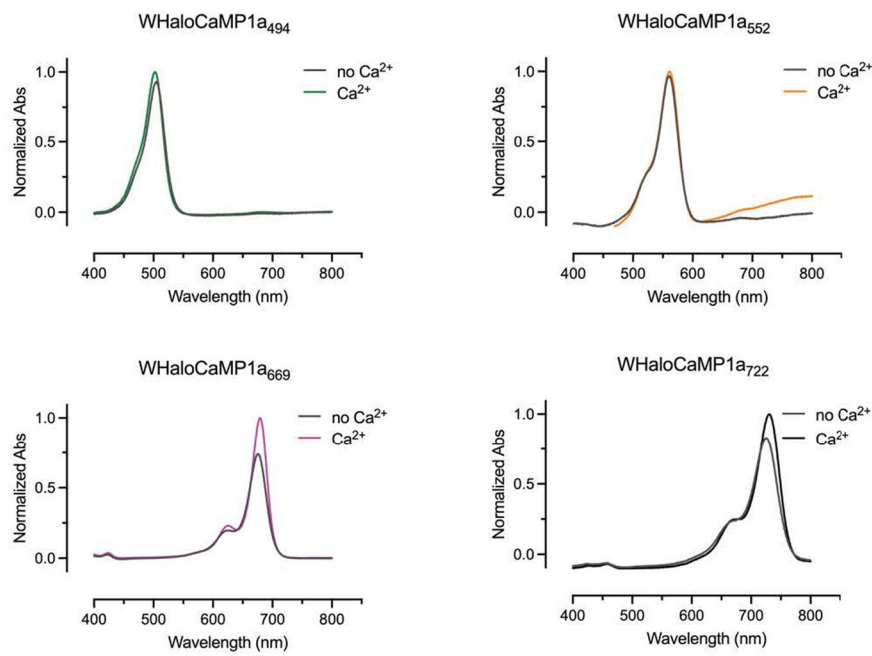
Round 1: single site saturations on top of insertion at site Delta T155 MLCK -(GGS)₄-CaM
Delta D156 with A151W: G158X, K160X, L161X, R153X, T154X, V157X, Q165X.

Mutation	Calc k_2 (M⁻¹ s⁻¹) EGTA	Calc k_2 (M⁻¹ s⁻¹) Ca^{2+}	$\Delta F/F_0$	EC ₅₀ (nM)	Hill
V157K	Over 10^6	$1 \times 10^5 \pm 1 \times 10^4$	0.5 ± 0.2		
G158D (WHaloCaMP1b)	$9 \times 10^4 \pm 7 \times 10^3$	$1 \times 10^4 \pm 3 \times 10^3$	2.5 ± 0.4	145 ± 6	3.7 ± 0.5

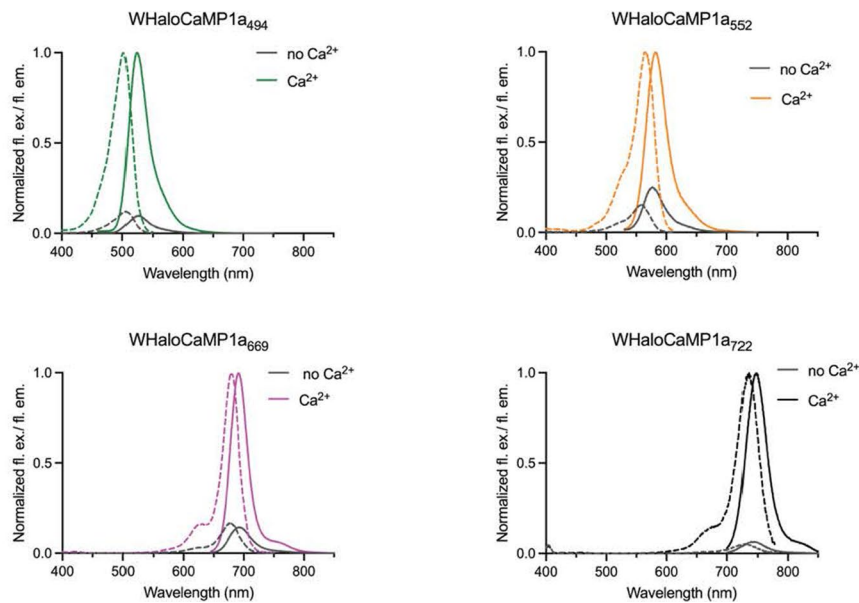
Extended Data Fig. 7 | Design and characterization of WHaloCaMP1b. **a.** The MLCK CaM-binding peptide and CaM were inserted at HaloTag T154, deleting T155 and D156. One round of single site saturation mutagenesis produced hits with improved calcium response (G158D). Further rounds of directed evolution did not give better variants. **b.** Crystal structure of HaloTag7₆₆₉ highlighting relevant positions. **c.** $\Delta F/F_0$ vs. $[Ca^{2+}]$ of WHaloCaMP1b₆₆₉. Titrations are plotted as

the mean and s.d. of three technical replicates. **d.** Stopped-flow Ca^{2+} kinetics of unbinding for WHaloCaMP1b₆₆₉. **e.** Representative trace (black) from one run of the field stimulation assay with ~40 neuron ROIs. Grey trace is standard error of the mean (s.e.m.) of the fluorescence trace. F_0 was calculated 1 s before the first field stimulus. The table reports fits from experiments in panels **c**.

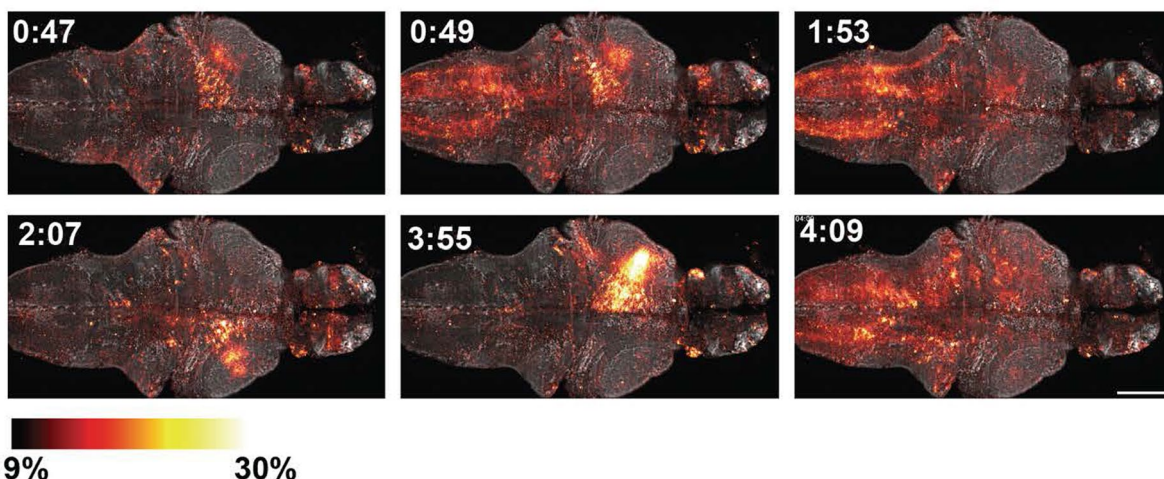
a.



b.

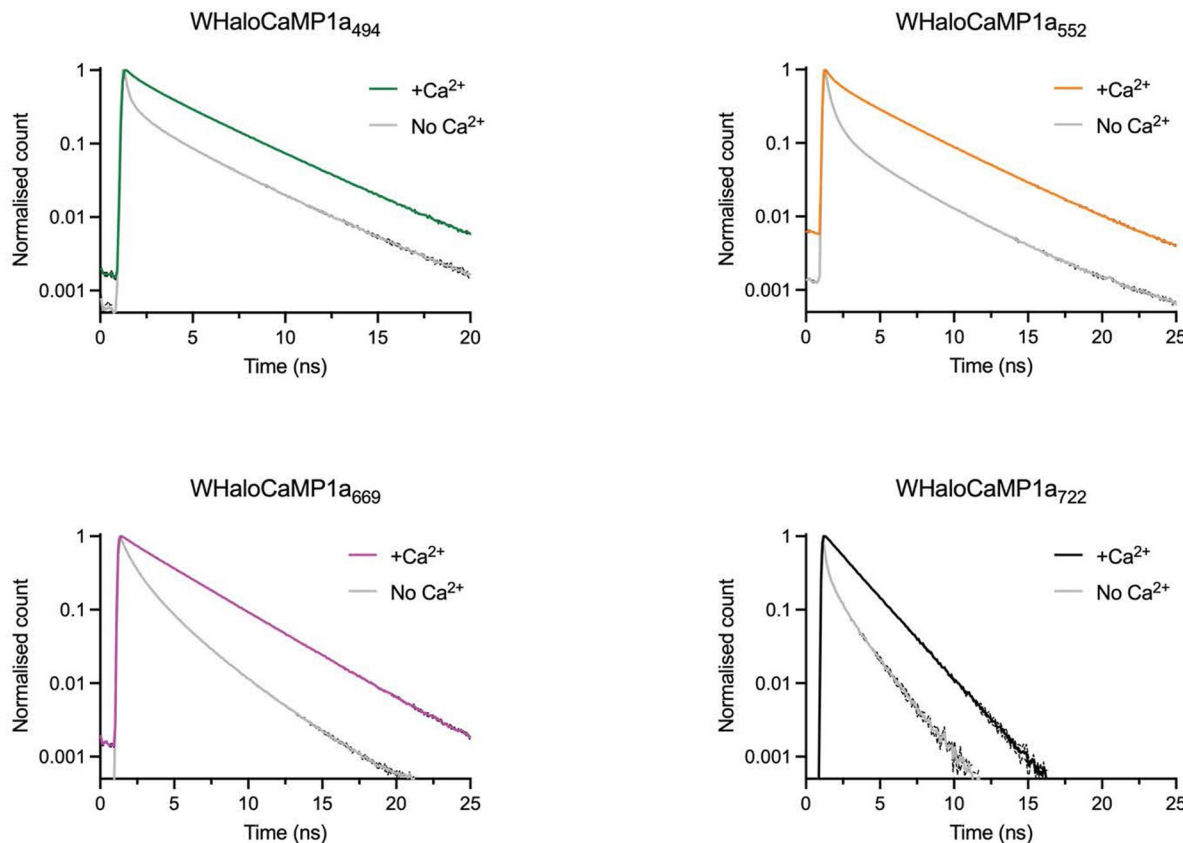


Extended Data Fig. 8 | Absorption and fluorescence spectra for WHaloCaMP1a. WHaloCaMP1a bound to JF₄₉₄-HaloTag ligand, JF₅₅₂-HaloTag ligand, JF₆₆₉-HaloTag ligand and JF₇₂₂-HaloTag ligand. Absorption (a.) and fluorescence excitation and emission spectra (b.). Spectra were normalized to max absorbance or fluorescence excitation or emission in the Ca^{2+} state.



Extended Data Fig. 9 | Volumetric whole brain imaging of neurons in zebrafish larvae using SiMView. Tg(*elavl3*:NES-WHaloCaMP1a-EGFP) zebrafish were labeled with JF₆₆₉-HaloTag ligand and mounted in a SiMView light sheet microscope. Three-dimensional volumes of the brain with a 160 μm length along the z-axis were acquired with a z-step size of 4 μm and a rate of 4 volumes

per second. Visualization of $\Delta F/F_0$ (shown using a red-hot color look-up table) displayed over a projection of the concatenated projected $\Delta F/F_0$ time series that serves as an anatomical reference (shown in grey). Time stamps are in min:s and scale bar is 100 μm . A movie of this whole brain time-lapse image data set can be found in Supplementary Movie 1.



	Ca ²⁺ lifetime (ns)	EGTA lifetime (ns)	Delta lifetime (ns)
WHaloCaMP1a ₄₉₄	2.89 ± 0.03	0.73 ± 0.01	2.02
WHaloCaMP1a ₅₅₂	2.87 ± 0.03	0.86 ± 0.01	2.15
WHaloCaMP1a ₆₆₉	3.43 ± 0.04	1.27 ± 0.01	2.15
WHaloCaMP1a ₇₂₂	1.87 ± 0.01	0.49 ± 0.01	1.34
iGECI	1.13 ± 0.01	1.11 ± 0.01	0.02

Extended Data Fig. 10 | Fluorescence lifetimes of WHaloCaMP1a and iGECI.

Fluorescence lifetime image microscopy (FLIM) with WHaloCaMP1a bound to JF₄₉₄-HaloTag ligand, JF₅₅₂-HaloTag ligand, JF₆₆₉-HaloTag ligand or JF₇₂₂-HaloTag ligand, and iGECI. A time domain FLIM set-up was used at 40 MHz. The lifetime

decay was fit to a three-component fit for WHaloCaMP1a. A two component fit was performed for iGECI. No additional biiverdin was added to the iGECI sample before imaging. The amplitude weighted lifetime is reported. Mean and standard deviation from three replicates from at least two different samples.

Reporting Summary

Nature Portfolio wishes to improve the reproducibility of the work that we publish. This form provides structure for consistency and transparency in reporting. For further information on Nature Portfolio policies, see our [Editorial Policies](#) and the [Editorial Policy Checklist](#).

Statistics

For all statistical analyses, confirm that the following items are present in the figure legend, table legend, main text, or Methods section.

n/a Confirmed

- The exact sample size (n) for each experimental group/condition, given as a discrete number and unit of measurement
- A statement on whether measurements were taken from distinct samples or whether the same sample was measured repeatedly
- The statistical test(s) used AND whether they are one- or two-sided
Only common tests should be described solely by name; describe more complex techniques in the Methods section.
- A description of all covariates tested
- A description of any assumptions or corrections, such as tests of normality and adjustment for multiple comparisons
- A full description of the statistical parameters including central tendency (e.g. means) or other basic estimates (e.g. regression coefficient) AND variation (e.g. standard deviation) or associated estimates of uncertainty (e.g. confidence intervals)
- For null hypothesis testing, the test statistic (e.g. F , t , r) with confidence intervals, effect sizes, degrees of freedom and P value noted
Give P values as exact values whenever suitable.
- For Bayesian analysis, information on the choice of priors and Markov chain Monte Carlo settings
- For hierarchical and complex designs, identification of the appropriate level for tests and full reporting of outcomes
- Estimates of effect sizes (e.g. Cohen's d , Pearson's r), indicating how they were calculated

Our web collection on [statistics for biologists](#) contains articles on many of the points above.

Software and code

Policy information about [availability of computer code](#)

Data collection

The Cary Model 100 spectrometer was controlled by CaryWinUV 4.20(468) software. The Cary Eclipse was controlled by Cary Eclipse Scan Application 1.1(132) software. The Quantaurus Quantum Yield spectrophotometer was controlled by PLQY software U6039-05 3.4.2. The Zeiss Lightsheet Z.1 was controlled by Zen. The Leica STELLARIS 8 FALCON microscope was controlled by Leica Application Suite X. The Nikon Eclipse Ti microscope was controlled by NIS-Elements AR 4.40.0, 64-bit (build 1084) software. Scanimate was implemented in MATLAB R2020b for image acquisitions. Wavesurfer Version 1.0.0.0 was also used implemented via MATLAB R2020b. μManager Version 1.4. The plate reader was run via Tecan Sparkcontrol method editor v. 3.0.

Data analysis

Data analysis was performed in Microsoft Excel Version 16.85 and MATLAB 2012b and R2023B. Snapgene v. 7.2.1. was used to design constructs. Image analysis was performed in FIJI v. 2.14.0/1.54f and Leica LASX FLIM/FCS software. GraphPad Prism software v. 10.2.3 was used for data representation, curve fitting and statistical tests. Neuronal activity was analyzed using suite2p, Cellpose and Rastermap. The protein-dye structure was solved in the CCP4 suite, using Xia2/DIALS, scala, PHASER, REFMAC5 and Coot.

For manuscripts utilizing custom algorithms or software that are central to the research but not yet described in published literature, software must be made available to editors and reviewers. We strongly encourage code deposition in a community repository (e.g. GitHub). See the Nature Portfolio [guidelines for submitting code & software](#) for further information.

Data

Policy information about [availability of data](#)

All manuscripts must include a [data availability statement](#). This statement should provide the following information, where applicable:

- Accession codes, unique identifiers, or web links for publicly available datasets
- A description of any restrictions on data availability
- For clinical datasets or third party data, please ensure that the statement adheres to our [policy](#)

The authors declare that the source data used to generate the figures in this manuscript are available from the Figshare repository: <https://doi.org/10.25378/janelia.25934782>. The structure of HaloTag7 bound to JF669 has been deposited to the Protein Data Bank (PDBID = 8SW8).

DNA plasmids encoding WHaloCaMP used in this work are available from Addgene as follows:

205303 pRSET-WHaloCaMP1a-EGFP
 205304 pRSET-WHaloCaMP1a
 205305 pRSET-WHaloCaMP1b-EGFP
 205306 pRSET-WHaloCaMP-eNOSpep-EGFP
 205307 pAAV-synapsin-WHaloCaMP1a-EGFP
 205308 pAAV-synapsin-WHaloCaMP1a
 205309 pAAV-CaMKII-WHaloCaMP1a-EGFP
 205310 pAAV-CaMKII-WHaloCaMP1a
 205311 pTol2-elavl3-WHaloCaMP1a-EGFP
 205312 pTol2-elavl3-WHaloCaMP1a

Human research participants

Policy information about [studies involving human research participants and Sex and Gender in Research](#).

Reporting on sex and gender

N/A

Population characteristics

N/A

Recruitment

N/A

Ethics oversight

N/A

Note that full information on the approval of the study protocol must also be provided in the manuscript.

Field-specific reporting

Please select the one below that is the best fit for your research. If you are not sure, read the appropriate sections before making your selection.

Life sciences

Behavioural & social sciences

Ecological, evolutionary & environmental sciences

For a reference copy of the document with all sections, see nature.com/documents/nr-reporting-summary-flat.pdf

Life sciences study design

All studies must disclose on these points even when the disclosure is negative.

Sample size

No specific sample size calculations were performed. Generally, sample size was the maximum possible within reasonable time and resource application limits.

Data exclusions

No data was excluded from analysis.

Replication

All attempts at replication were successful. Number of replications for each experiment are described in the methods, figure captions and/or main text.

Randomization

Where appropriate for comparative analysis, samples were randomly allocated into experimental groups.

Blinding

No blinding was performed, primarily to reduce experimental complexity as no novel comparative experiments were central to the conclusions of this work.

Reporting for specific materials, systems and methods

We require information from authors about some types of materials, experimental systems and methods used in many studies. Here, indicate whether each material, system or method listed is relevant to your study. If you are not sure if a list item applies to your research, read the appropriate section before selecting a response.

Materials & experimental systems

n/a	<input checked="" type="checkbox"/> Involved in the study
<input checked="" type="checkbox"/>	Antibodies
<input type="checkbox"/>	Eukaryotic cell lines
<input checked="" type="checkbox"/>	Palaeontology and archaeology
<input type="checkbox"/>	Animals and other organisms
<input checked="" type="checkbox"/>	Clinical data
<input checked="" type="checkbox"/>	Dual use research of concern

Methods

n/a	<input checked="" type="checkbox"/> Involved in the study
<input checked="" type="checkbox"/>	ChIP-seq
<input checked="" type="checkbox"/>	Flow cytometry
<input checked="" type="checkbox"/>	MRI-based neuroimaging

Eukaryotic cell lines

Policy information about [cell lines](#) and [Sex and Gender in Research](#)

Cell line source(s)	HeLa cells (CCL-2) were purchased from ATCC.
Authentication	No authentication of the cell line was performed.
Mycoplasma contamination	Cells were regularly tested by Janelia Cell Culture Facility and were negative.
Commonly misidentified lines (See ICLAC register)	No commonly misidentified cell lines were used in this study.

Animals and other research organisms

Policy information about [studies involving animals](#); [ARRIVE guidelines](#) recommended for reporting animal research, and [Sex and Gender in Research](#)

Laboratory animals	Adult C57/BL6 male mice, 2-4 months old. Emx1IRES cre mice (JAX #005628 strain) and FLIM-AKAR mice (JAX #039003), both C57/BL6 background, P15-P19. Rattus norvegicus (rat), Sprague-Dawley, 0-1 days. Zebra fish larvae was of the species Danio rerio and were transgenic and used at 4-6. d.p.f. Flies were of the species Drosophila melanogaster and used 2-10 days progeny of a heterozygous cross of drivers and WHaloCaMP variants.
Wild animals	No wild animals were used in this study.
Reporting on sex	The gender of zebrafish larvae cannot be determined, thus sex was not considered in the experimental design. Flies (adult, females) were used. Male mice were used for imaging WHaloCaMP in the visual cortex. For the slice experiments in mice, the sex of the mice was not determined.
Field-collected samples	No field-collected samples were used.
Ethics oversight	Experimental protocols were conducted according to the National Institutes of Health guidelines for animal research and were approved by the Institutional Animal Care and Use Committee at the Janelia Research Campus, HHMI, Institutional Animal Care and Use Committee at University of Maryland Baltimore, and Washington University Institutional Animal Care and Use Committee.

Note that full information on the approval of the study protocol must also be provided in the manuscript.